B-meson signatures of a supersymmetric U(2) flavor model

Shrihari Gopalakrishna[*],[†] and C.-P. Yuan[‡]

Department of Physics and Astronomy, Michigan State University, East Lansing, Michigan 48824, USA
(Received 14 December 2004; published 16 February 2005)

We discuss *B*-meson signatures of a Supersymmetric U(2) flavor model, with relatively light (electroweak scale masses) third generation right-handed scalars. We impose current *B* and *K* meson experimental constraints on such a theory, and obtain expectations for $B_d \to X_s \gamma$, $B_d \to X_s g$, $B_d \to X_s \ell^+ \ell^-$, $B_d \to \phi K_s$, $B_s \bar{B}_s$ mixing and the dilepton asymmetry in B_s. We show that such a theory is compatible with all current data, and furthermore, could reconcile the apparent deviations from Standard Model predictions that have been found in some experiments.

I. INTRODUCTION

The Standard Model (SM) of high energy physics suffers from the gauge hierarchy problem and the flavor problem. The first is the fine tuning required to maintain a low electroweak mass scale (M_{EW}) in the theory, in the presence of a high scale, the Planck Scale (M_{Pl}). The second problem is a lack of explanation of the mass hierarchy and mixings of the quarks and leptons.

Supersymmetry (SUSY) eliminates the gauge hierarchy problem by introducing for each SM particle, a new particle with the same mass but different spin. For example, for each SM quark/lepton a new scalar (squark/slepton), and for each SM gauge boson a new fermion (gaugino), is introduced. If SUSY is realized in nature, the fact that we do not see such new particles, we believe, could be because SUSY is spontaneously broken, making the superpartners heavier than the mass ranges probed by experiments. Owing to a lack of understanding of how exactly SUSY is broken, a phenomenologically general Lagrangian, for example, the Minimal Supersymmetric Standard Model (MSSM), is usually considered to compare with data. Various experimental searches have placed constraints on the masses and couplings in the MSSM.

Attempts have been made to address the flavor problem by proposing various flavor symmetries. In a supersymmetric theory, a flavor symmetry in the quark sector might imply a certain structure in the scalar sector, leading to definite predictions for flavor changing neutral current (FCNC) processes on which experiments have placed severe constraints. In the literature, a lot of attention has been devoted toward analyzing the minimal flavor violation (MFV) scenario, in which the scalar flavor structure is aligned with the quark sector so that the two are simultaneously diagonalized. In MFV, the Cabibbo-Kobayashi-Maskawa (CKM) quark-mixing matrix describes the flavor changing interactions in the supersymmetric sector as well,

and the only CP violating phase is the one in the CKM matrix. In this work, we do not assume such an alignment, and we will consider nonminimal flavor violation (NMFV), which we treat as a perturbation over the MFV case.

In this paper we wish to explore in what form a supersymmetric extension of the SM, with a U(2) flavor symmetry, could influence *K* and *B* physics observables. We thus restrict ourselves to the quark and scalar-quark (squark) sectors. We consider an "effective supersymmetry" [1] framework, with heavy (TeV scale) first two generation squarks, in order to escape neutron electric dipole moment (EDM) constraints. This allows the possibility of having large CP violating phases in the squark sector. We consider a supersymmetric U(2) theory [2,3], impose recent *K* and *B* meson experimental constraints and obtain predictions for $B_d \to X_s \gamma$, $B_d \to X_s g$, $B_d \to X_s \ell^+ \ell^-$, $B_d \to \phi K_s$, $B_s \bar{B}_s$ mixing and the dilepton asymmetry in B_s. Though we consider a specific flavor symmetry, namely, U(2), our conclusions would hold for any model with a sizable off-diagonal 32 element in the squark mass matrix.

Some *B* physics consequences in a supersymmetric U(2) theory have been considered in Ref. [3]. Large $\tan\beta$ effects in *B* decays have been carefully analyzed in Ref. [4], but for simplicity we will restrict ourselves to the case when $\tan\beta$ is not too large. Other work along similar lines, though in more general contexts, have been presented in Refs. [5–8]. In this work we will include all dominant contributions to a particular observable in order to include interference effects between various diagrams. This has not always been done in the literature. We will then study the implications of recent data from the B-factories, including the $b \to s$ penguin decay mode $B_d \to \phi K_s$ which shows a slight deviation from the SM prediction.

The paper is organized as follows: In Section II we specify the supersymmetric U(2) theory we will work with, and the choices we make for the various SUSY and SUSY breaking parameters. In Sections III and IV we consider $\Delta S = 2$ (Kaon mixing) and $\Delta B = 2$ ($B_d \bar{B}_d$ and $B_s \bar{B}_s$ mixing) FCNC process, respectively. In Section V we will consider the implications of such a theory to $\Delta B = 1$

*Current address: Dept. of Physics and Astronomy, Northwestern University, Evanston, IL 60208, USA
†Electronic address: shri@northwestern.edu
‡Electronic address: yuan@pa.msu.edu

FCNC processes, namely $B_d \to X_s\gamma$, $B_d \to X_sg$, $B_d \to X_s\ell^+\ell^-$ and $B_d \to \phi K_s$. We conclude in Section VI. We give details of various squark mixings and their diagonalization in Appendix A, and collect loop functions that we will need in Appendix B.

II. SUPERSYMMETRIC U(2)

A. The model

The supersymmetric model that we will discuss is as described in Ref. [3], with the first and second generation superfields (ψ_a, $a = 1, 2$) transforming as a U(2) doublet while the third generation superfield (ψ) is a singlet. The most general superpotential can be written as[1]:

$$\mathcal{W} = \psi\alpha_1 H\psi + \frac{\phi^a}{M}\psi\alpha_2 H\psi_a + \frac{\phi^{ab}}{M}\psi_a\alpha_3 H\psi_b$$
$$+ \frac{\phi^a\phi^b}{M^2}\psi_a\alpha_4 H\psi_b + \frac{S^{ab}}{M}\psi_a\alpha_5 H\psi_b + \mu H_u H_d, \tag{1}$$

where M is the cutoff scale below which such an effective description is valid, the α_i are O(1) constants, and three new U(2) tensor fields are introduced: ϕ^a a U(2) doublet, ϕ^{ab} a second rank antisymmetric U(2) tensor and S^{ab} a second rank symmetric U(2) tensor. The parameter μ could be complex and we allow for this possibility. Following Ref. [3], we assume that U(2) is broken spontaneously by the vacuum expectation value (VEV) [3][2]

$$\langle\phi^a\rangle = \begin{pmatrix} 0 \\ V \end{pmatrix}; \qquad \langle\phi^{ab}\rangle = v\epsilon^{ab}; \qquad \langle S^{11,12,21}\rangle = 0,$$
$$\langle S^{22}\rangle = V, \tag{2}$$

with $V/M \equiv \epsilon \sim 0.02$ and $v/M \equiv \epsilon' \sim 0.004$, in order to get the correct quark masses. These VEV's lead to the quark mass matrix given by (we show only the down quark mass matrix after the $SU(2)_L$ is broken by the usual Higgs mechanism)

$$\mathcal{L} \supset -\bar{d}_R\,\bar{s}_R\,\bar{b}_R\,\mathcal{M}_d\begin{pmatrix} d_L \\ s_L \\ b_L \end{pmatrix} + \text{h.c.}, \tag{3}$$

---

[1]In the superpotential each term encodes the "vertical" gauge symmetry, which, at the weak scale, is $SU(3) \times SU(2) \times U(1)$. Thus ($i, j$ labels generations),

$$\psi_i\alpha H\psi_j \equiv \alpha_u Q_i U_j^c H_u + \alpha'_u U_i^c Q_j H_u + \alpha_d Q_i D_j^c H_d$$
$$- \alpha'_d D_i^c Q_j H_d + (\text{Lepton sector}).$$

[2]The dynamical means by which this VEV is generated is left unspecified. In general, $\langle S^{22}\rangle$ can be different from $\langle\phi^a\rangle$, but for simplicity we will assume that they are the same. Also for simplicity, we take ϵ, ϵ' to be real.

$$\mathcal{M}_d = v_d\begin{pmatrix} O & -\lambda_1\epsilon' & O \\ \lambda_1\epsilon' & \lambda_2\epsilon & \lambda_4\epsilon \\ O & \lambda'_4\epsilon & \lambda_3 \end{pmatrix},$$

where $v_d = \langle h_d\rangle$ is the VEV of the Higgs field. In $\mathcal{M}_d$, the λ_i's are O(1) (complex) coefficients, given in terms of the α_i's. Ref. [3] shows that such a pattern of the mass matrix explains the quark masses and CKM elements.

If U(2) is still a good symmetry at the SUSY breaking scale, and broken (spontaneously) only below the SUSY breaking scale, the SUSY breaking terms would have a structure dictated by U(2). For our purposes it is sufficient to consider the down sector squark mass matrices, and they are given as

$$\mathcal{L} \supset -\tilde{d}_L^*\tilde{s}_L^*\tilde{b}_L^*\mathcal{M}_{LL}^2\begin{pmatrix} \tilde{d}_L \\ \tilde{s}_L \\ \tilde{b}_L \end{pmatrix} - (\tilde{d}_R^*\tilde{s}_R^*\tilde{b}_R^*)\mathcal{M}_{RR}^2\begin{pmatrix} \tilde{d}_R \\ \tilde{s}_R \\ \tilde{b}_R \end{pmatrix}$$
$$+ \left[(\tilde{d}_R^*\tilde{s}_R^*\tilde{b}_R^*)\mathcal{M}_{RL}^2\begin{pmatrix} \tilde{d}_L \\ \tilde{s}_L \\ \tilde{b}_L \end{pmatrix} + \text{h.c.}\right], \tag{4}$$

$$\mathcal{M}_{LL}^2 = \mathcal{M}_d^\dagger\mathcal{M}_d + \begin{pmatrix} m_1^2 & i\epsilon'm_5^2 & 0 \\ -i\epsilon'm_5^2 & m_1^2 + \epsilon^2 m_2^2 & \epsilon m_4^{2*} \\ 0 & \epsilon m_4^2 & m_3^2 \end{pmatrix}_{LL}$$
$$+ \text{D} - \text{term},$$

$$\mathcal{M}_{RR}^2 = \mathcal{M}_d\mathcal{M}_d^\dagger + \begin{pmatrix} m_1^2 & i\epsilon'm_5^2 & 0 \\ -i\epsilon'm_5^2 & m_1^2 + \epsilon^2 m_2^2 & \epsilon m_4^{2*} \\ 0 & \epsilon m_4^2 & m_3^2 \end{pmatrix}_{RR}$$
$$+ \text{D} - \text{term},$$

$$\mathcal{M}_{RL}^2 = \mu^*\tan\beta\mathcal{M}_d + v_d\begin{pmatrix} O & -A_1\epsilon' & O \\ A_1\epsilon' & A_2\epsilon & A_4\epsilon \\ O & A'_4\epsilon & A_3 \end{pmatrix}, \tag{5}$$

where m_i^2 and A_i are determined by the SUSY breaking mechanism. Here m_1^2, m_2^2, m_3^2 and m_5^2 are real, while m_4^2 and A_i could be complex. We will assume that the A_i are of order A, a common mass scale. The D terms are flavor diagonal, and since we are interested in FCNC processes, we will not write them in detail, but will think of them as included in m_1^2 and m_3^2.

Thus far we have presented the mass matrices in the gauge basis. In the following sections, we will work in the superKM basis in which the quark mass matrix is diagonal, and the quark field rotations that diagonalize the quark mass matrix are applied to the squarks, whose mass matrix would also have been diagonalized in the MFV scheme. Since we will not assume an MFV structure, in the superKM basis, there would be small off-diagonal terms in the squark mass matrix, which we treat as perturbations. The structure of the squark mass matrix in the superKM

basis is similar to that in Eq. (5) owing to the smallness of the mixing angles that diagonalize the quark mass matrix.

B. SUSY parameters

Lacking specific knowledge about the SUSY breaking mechanism realized in nature, we make some assumptions on the SUSY mass spectrum. Neutron EDM places strong constraints on the CP violating phases and the masses of the first two generations of scalars. To satisfy this and other collider constraints, we consider an "effective SUSY" framework in which the scalars of the first two generations are heavy, suppressing EDM, and allowing for larger CP violating phases. Defining the scalar mass scale, $m_0 \sim$ 1 TeV, we take all $m_i \sim m_0$ except for $m_{\tilde{t}_R, \tilde{b}_R} \equiv m_{3RR} \sim$ 100 GeV. We take $A \sim m_0$, the gaugino mass parameter M_2 and charged-Higgs masses to be 250 GeV and the gluino mass to be 300 GeV.[3] We assume such a spectrum just above the weak scale without specifying what mechanism of SUSY breaking and mediation might actually give rise to it. As we will show later, if realized in nature such a spectrum would lead to enhancements in the processes we are considering here.

The rates of various FCNC processes follow from the mass matrix that we have specified in Eq. (5). We will work in the superKM basis. The interaction vertices in the mass basis are obtained by diagonalizing the mass matrices in Eq. (5), and the perturbative diagonalization to leading order is shown in Appendix A.

The dominant NMFV SUSY contributions to FCNC processes would be due to the 32 and 23 entries in Eq. (5), since they are the biggest off-diagonal terms. For convenience we define

$$\delta_{32,23}^{RL,RR,LL} \equiv \frac{(\mathcal{M}^2_{RL,RR,LL})_{32,23}}{m_0^2}. \tag{6}$$

Since we have written down an effective theory and not specified the dynamics of U(2) and SUSY breaking, we can only specify the order of magnitude of $\delta_{32,23}$. To parametrize this uncertainty we write,

$$\delta_{32,23}^{RL} = \frac{v_d A \epsilon}{m_0^2} d_{32,23}^{RL}, \qquad \delta_{32,23}^{LL,RR} = \frac{\epsilon m_4^2}{m_0^2} d_{32,23}^{LL,RR}, \tag{7}$$

where we have denoted the unknown $\mathcal{O}(1)$ coefficients by $d_{32,23}^{LL,RR,RL}$.

We summarize our choice of the parameters in Table I. For these values, from Eq. (7), the natural sizes of $\delta_{32,23}$ are given by

$$\delta_{32,23}^{RL} = 6.82 \times 10^{-4} d_{32,23}^{RL}, \qquad \delta_{32,23}^{LL,RR} = 0.02 d_{32}^{LL,RR}. \tag{8}$$

---

[3]The Tevatron bounds on the stop, sbottom and gluino masses are discussed in Ref. [9]. We note here that the bounds in general get less stringent as the neutralino mass increases.

TABLE I. Default SUSY parameters for this work that satisfy all experimental constraints discussed in this paper. All masses are in GeV.

m_0	1000	$\tan\beta$	5
$m_{\tilde{b}_R, \tilde{t}_R}$	100	μ	$200e^{i2.2}$
$m_{\tilde{d}_R, \tilde{s}_R}$	1000	M_2	250
$m_{\tilde{q}_L}$	1000	$M_{\tilde{g}}$	300
A	1000	$m_{H^\pm}$	250
d_{32}^{RL}	$2e^{i3.2}$	d_{32}^{RR}	$1.75e^{i1.6}$

We will find in the rest of this paper that δ^{RL} induces NMFV $\Delta B = 1$ FCNC processes dominantly, while $\delta^{RR,LL}$ induces $\Delta S = 2$ and $\Delta B = 2$ FCNC processes. Though the δ_{32}^{RL} and δ_{23}^{RL} elements have similar magnitudes, the δ_{32}^{RL} gluino NMFV contribution to $\Delta B = 1$ FCNC processes is larger, since we take $\tilde{b}_R$ to be much lighter than the other scalars, and the δ_{23}^{RL} gluino diagrams are relatively suppressed by the heavier $\tilde{b}_L$ mass. Therefore, in this work we will include only the dominant δ_{32}^{RL} contribution. We illustrate this in Fig. 1, where we show the gluino contribution to $B_d \rightarrow X_s \gamma$ as an example. Similarly, owing to the smaller $\tilde{b}_R$ mass, the $\delta_{32,23}^{RR}$ NMFV contribution to $\Delta S = 2$ and $\Delta B = 2$ FCNC processes is relatively larger compared to the $\delta_{32,23}^{LL}$ contribution. We note here that, from Eq. (A11) in Appendix A, the sbottom mixing angle is negligibly small, and therefore, we ignore sbottom mixing effects; stop mixing is not as small and we include its effects.

In the next three sections we will discuss the implication of the U(2) model to $\Delta S = 2$, $\Delta B = 2$ and $\Delta B = 1$ FCNC processes. From this we will see that present experimental data are compatible with the values shown in Table I, and we will obtain expectations for some measurements that are forthcoming. We will present plots of different FCNC effects by varying a couple of parameters at a time, while keeping all others fixed at the values shown in Table I.

III. $\Delta S = 2$ FCNC PROCESS

The CP violation parameter ϵ_K due to mixing in the Kaon sector has been measured to be [10]

$$|\epsilon_K| = (2.284 \pm 0.014) \times 10^{-3}. \tag{9}$$

We wish to estimate the new physics contributions to ϵ_K in the scenario that we are considering. Here we note that even though the direct CP violation parameter ϵ_K'/ϵ_K has also been measured, large hadronic uncertainties do not permit us to constrain new physics models through this observable.

Kaon mixing is governed by the $\Delta S = 2$ effective Hamiltonian

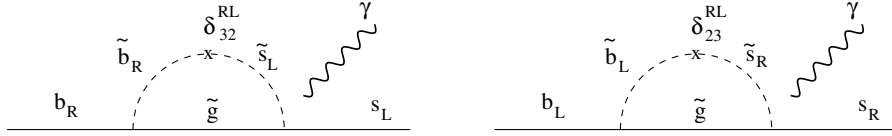$$\mathcal{H}_{\Delta S=2}^{\text{eff}} = \sum_{i=1}^{5} C_i Q_i + \sum_{i=1}^{3} \tilde{C}_i \tilde{Q}_i, \tag{10}$$

FIG. 1.   Gluino contribution to $B_d \to X_s\gamma$. The diagram on the left, proportional to δ^{RL}_{32}, has the lighter scalar $\tilde{b}_R$, while the one on the right, proportional to δ^{RL}_{23}, only has heavier scalars and is therefore relatively suppressed.

where,

$$Q_1 = \bar{d}^\alpha_L \gamma_\mu s^\alpha_L \bar{d}^\beta_L \gamma^\mu s^\beta_L, \qquad Q_2 = \bar{d}^\alpha_R s^\alpha_L \bar{d}^\beta_R s^\beta_L,$$

$$Q_3 = \bar{d}^\alpha_R s^\beta_L \bar{d}^\beta_R s^\alpha_L, \qquad Q_4 = \bar{d}^\alpha_R s^\beta_L \bar{d}^\beta_L s^\beta_R, \qquad (11)$$

$$Q_5 = \bar{d}^\alpha_R s^\beta_L \bar{d}^\beta_L s^\alpha_R.$$

The operators $\tilde{Q}_i(i = 1, 2, 3)$ are obtained by exchanging $L \leftrightarrow R$. In the SM and the new physics model we are considering, the dominant contributions are to Q_1, as we explain later in this section. The CP violation parameter ϵ_K is then given by (see, for example, Ref. [11])

$$\epsilon_K = e^{i\pi/4} \frac{1}{3\sqrt{2}} \frac{m_K B_K f_K^2}{\Delta m_K} \text{Im}[C_1(m_K)], \qquad (12)$$

where B_K is the Bag parameter and f_K is the Kaon decay constant.

In addition to the SM W box diagram contribution to C_1, in the supersymmetric U(2) theory we are considering, the charged-Higgs and chargino MFV contributions could be sizable. The dominant MFV contributions to C_1 can be written as

$$C_1^{\text{MFV}} = C_1^W + C_1^H + C_1^\chi, \qquad (13)$$

which is the sum of the SM W, the charged-Higgs, and the chargino contributions, respectively.

SM contribution.—The SM W contribution is [12]

$$C_1^{\text{SM}}(m_t) = C_1^W(m_t)$$
$$= \frac{G_F^2 m_W^2}{4\pi^2} \{ (V_{td}^* V_{ts})^2 S_0(x_t). + (V_{cd}^* V_{cs})^2 S_0(x_c)$$
$$+ 2(V_{td}^* V_{ts} V_{cd}^* V_{cs}) S_0(x_t, x_c) \}, \qquad (14)$$

where the function S_0 is given in Appendix B, Eq. (B3), and $x_t \equiv m_t^2/m_W^2$, $x_c \equiv m_c^2/m_W^2$. The QCD correction due to renormalization group running from m_t to m_b gives

$$C_1^{\text{SM}}(m_K) = C_1^W(m_K)$$
$$= \frac{G_F^2 m_W^2}{4\pi^2} \{ (V_{td}^* V_{ts})^2 \eta_{K33} S_0(x_t).$$
$$+ (V_{cd}^* V_{cs})^2 \eta_{K22} S_0(x_c)$$
$$+ 2(V_{td}^* V_{ts} V_{cd}^* V_{cs}) \eta_{K32} S_0(x_t, x_c) \}, \qquad (15)$$

where the η_K are QCD correction factors given in Eq. (20) below, and V_{ij} are the CKM matrix elements.

Charged-Higgs contribution.—Supersymmetric theories require two Higgs doublets to give masses to the up and down type fermions. The Higgs doublets contain the charged-Higgs $H^\pm$, and the dominant charged-Higgs-top contribution is [11][4]

$$C_1^H(m_t) = \frac{G_F^2 m_W^2}{4\pi^2} (V_{td}^* V_{ts})^2 [-F_V^H],$$

$$F_V^H = \frac{1}{4\tan^4\beta} x_t^2 Y_1(r_H, r_H, x_t, x_t)$$
$$+ \frac{1}{2\tan^2\beta} x_t^2 Y_1(1, r_H, x_t, x_t) \qquad (16)$$
$$- \frac{2}{\tan^2\beta} x_t Y_2(1, r_H, x_t, x_t),$$

where $r_H \equiv m_H^2/m_W^2$, and the functions Y_1 and Y_2 are given in Appendix B, Eq. (B4).

Chargino contribution.—The dominant chargino-right-handed-stop contribution is [11]

$$C_1^\chi(m_t) = \frac{G_F^2 m_W^2}{4\pi^2} (V_{td}^* V_{ts})^2 [-F_V^\chi],$$
$$F_V^\chi = \frac{1}{4} |\Gamma^{(i)}_{\chi R}|^2 |\Gamma^{(j)}_{\chi R}|^2 Y_1(r_{\tilde{t}_2}, r_{\tilde{t}_2}, s_i, s_j), \qquad (17)$$

where $r_{\tilde{t}_2} \equiv m_{\tilde{t}_2}^2/m_W^2$, $s_{1,2} \equiv m_{\tilde{\chi}_{1,2}}^2/m_W^2$, and the coupling is given by

$$\Gamma^{(i)}_{\chi R} = \sqrt{2}(C_R^*)_{1i}(C_{\tilde{t}}^*)_{12} - \frac{(C_R^*)_{2i}(C_{\tilde{t}}^*)_{22}}{\sin\beta} \frac{m_t}{m_W}, \qquad (18)$$

with the chargino and stop diagonalization matrices (C_R) and $(C_{\tilde{t}})$ given in Appendix A, Eqs. (A6) and (A10), respectively . Taking into account renormalization group running, we have

$$C_1^{H,\chi}(m_K) \approx \eta_{K33} C_1^{H,\chi}(m_t). \qquad (19)$$

Gluino contribution.—In general, the NMFV gluino contributions induce many operators shown in Eq. (11), but in the model we are considering, these are not significant due to a suppression from the heavy $\tilde{d}$ and $\tilde{s}$ masses, Glashow-Iliopoulos-Maiani (GIM) suppression owing to their approximate degeneracy (split only by $\mathcal{O}(\epsilon^2)$ cf. Equation (5)), and the contribution from the relatively light

---

[4]The charged-Higgs also contributes to the operator $\tilde{Q}_2$, which becomes important only at large $\tan\beta$.

right-handed-sbottom being suppressed by its small mixing to the first two generations. Moreover, owing to the structure of the mass matrix, Eq. (5), the gluino contribution is real, and hence does not contribute to ϵ_K.

In our numerical analysis, we take the following values for the various parameters [10,12]:

$$\eta_{K33} = 0.57, \qquad \eta_{K22} = 1.38, \qquad \eta_{K32} = 0.47,$$
$$f_K = 0.160 \text{ GeV}, \qquad 0.6 < B_K < 0.9,$$
$$m_K = 0.497 \text{ GeV}, \qquad (20)$$
$$\Delta m_K = (3.48 \pm 0.01) \times 10^{-15} \text{ GeV},$$
$$m_c = (1.2 \pm 0.2) \text{ GeV}.$$

The SM prediction for ϵ_K is in agreement with the experimental data, but it should be noted that there is considerable uncertainty in the lattice computation of the Bag parameter B_K (see Eq. (20)). The chargino and charged-Higgs contributions to C_1 add constructively with the SM contribution. Therefore, if the true value of B_K is taken to be closer to the lower limit, we can allow MFV contributions to be up by a factor of 1.2 compared to the SM value; i.e., $\text{Im}(C_1^{\text{MFV}})/\text{Im}(C_1^{\text{SM}}) \lesssim 1.2$. Figure 2 shows the region of MFV parameter space where this is satisfied. This justifies some of the choices we make in the list shown in Table I.
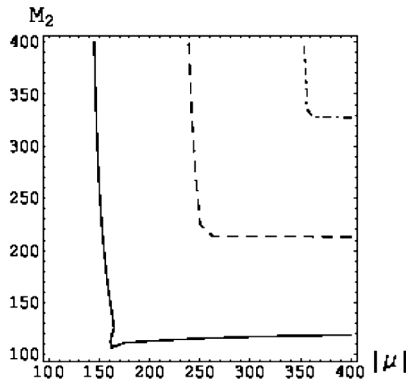
IV. $\Delta B = 2$ FCNC PROCESSES

A. General formalism

We start by discussing in general $B_q \bar{B}_q$ mixing and later specialize in succession to $B_d \bar{B}_d$ (q = d) and to $B_s \bar{B}_s$ (q = s). The $\Delta B = 2$ effective Hamiltonian is given by [13]:

$$\mathcal{H}_{\Delta B=2}^{\text{eff}} = \sum_{i=1}^{5} C_i Q_i + \sum_{i=1}^{3} \tilde{C}_i \tilde{Q}_i, \qquad (21)$$

where, for B_q,

$$Q_1 = \bar{q}_L^\alpha \gamma_\mu b_L^\alpha \bar{q}_L^\beta \gamma^\mu b_L^\beta, \qquad Q_2 = \bar{q}_R^\alpha b_L^\alpha \bar{q}_R^\beta b_L^\beta,$$
$$Q_3 = \bar{q}_R^\alpha b_L^\beta \bar{q}_R^\beta b_L^\alpha, \qquad Q_4 = \bar{q}_R^\alpha b_L^\alpha \bar{q}_L^\beta b_R^\beta, \qquad (22)$$
$$Q_5 = \bar{q}_R^\alpha b_L^\beta \bar{q}_L^\beta b_R^\alpha.$$

The operators $\tilde{Q}_i$ (i = 1, 2, 3) are obtained by exchanging $L \leftrightarrow R$. The Wilson coefficients C_i are run down from the SUSY scale, M_S, using [13]

$$C_r(m_b) = \sum_i \sum_s (b_i^{(r,s)} + \eta c_i^{(r,s)}) \eta^{a_i} C_s(M_S) \qquad (23)$$

where $\eta \equiv \alpha_s(M_S)/\alpha_s(m_t)$ and the a_i, b_i and c_i are constants given in Ref. [13].

The matrix elements of the Q_i in the vacuum insertion approximation are given by [13,14].

$$\langle \bar{B}_q | Q_1(\mu) | B_q \rangle = \frac{2}{3} m_{B_q}^2 f_{B_q}^2 B_1(\mu),$$

$$\langle \bar{B}_q | Q_2(\mu) | B_q \rangle = -\frac{5}{12} \left(\frac{m_{B_q}}{m_b + m_q} \right)^2 m_{B_q}^2 f_{B_q}^2 B_2(\mu),$$

$$\langle \bar{B}_q | Q_3(\mu) | B_q \rangle = \frac{1}{12} \left(\frac{m_{B_q}}{m_b + m_q} \right)^2 m_{B_q}^2 f_{B_q}^2 B_3(\mu), \qquad (24)$$

$$\langle \bar{B}_q | Q_4(\mu) | B_q \rangle = \frac{1}{2} \left(\frac{m_{B_q}}{m_b + m_q} \right)^2 m_{B_q}^2 f_{B_q}^2 B_4(\mu),$$

$$\langle \bar{B}_q | Q_5(\mu) | B_q \rangle = \frac{1}{6} \left(\frac{m_{B_q}}{m_b + m_q} \right)^2 m_{B_q}^2 f_{B_q}^2 B_5(\mu),$$

where we take for the decay constants $f_{B_q} = 0.2 \pm 0.03$ GeV and the Bag parameters (at scale m_b) $B_1 = 0.87$, $B_2 = 0.82$, $B_3 = 1.02$, $B_4 = 1.16$ and $B_5 = 1.91$ [13,14].

The B_q mass difference is given by

$$\Delta m_{B_q} = 2|M_{12}(B_q)|, \qquad (25)$$

where $M_{12}(B_q)$ is the off-diagonal Hamiltonian element for the $B_q \bar{B}_q$ system, and is given by

$$M_{12} = M_{12}^{\text{SM}} + M_{12}^{\text{SUSY}}, \qquad \Gamma_{12} \approx \Gamma_{12}^{\text{SM}}.$$
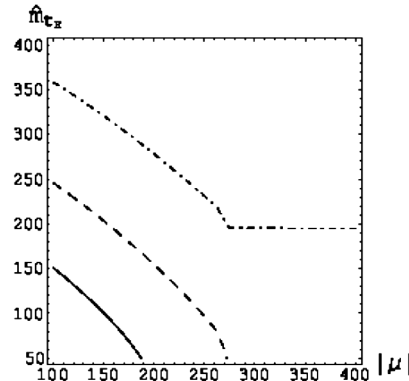

FIG. 2. The (dash-dot, dash, solid) curves are (1.05, 1.1, 1.2) contours of $\text{Im}(C_1^{\text{MFV}})/\text{Im}(C_1^{\text{SM}})$, showing the MFV contributions to Kaon mixing relative to the SM. Parameters not shown on a plot's axes are fixed as shown in Table I.

Γ_{12} to an excellent approximation is dominated by the SM tree decay modes. From Refs. [14,15] we have,

$$|M_{12}(B_q)| = \frac{1}{2m_{B_q}}|\langle B_q|\mathcal{H}^{\text{eff}}_{\Delta B=2}|\bar{B}_q\rangle|,$$

$$\Gamma_{12}^{\text{SM}} = (-1)\frac{G_F^2 m_b^2 m_{B_q} B_{B_q} f_{B_q}^2}{8\pi}\left\{v_t^2 + \frac{8}{3}v_c v_t\left(z_c + \frac{1}{4}z_c^2\right.\right.$$
$$\left.- \frac{1}{2}z_c^3\right) + v_c^2\left[\sqrt{1-4z_c}\left(1 - \frac{2}{3}z_c\right)\right.$$
$$\left.\left.+ \frac{8}{3}z_c + \frac{2}{3}z_c^2 - \frac{4}{3}z_c^3 - 1\right]\right\}, \quad (26)$$

where $v_x \equiv V_{xb}V_{xq}^*$, $z_c \equiv m_c^2/m_b^2$ and we take $B_{B_q} \approx 1.37$.

The dilepton asymmetry in B_q is given by [16]

$$A_{ll}^{B_q} \equiv \frac{N(B_q B_q) - N(\bar{B}_q\bar{B}_q)}{N(B_q B_q) + N(\bar{B}_q\bar{B}_q)} = \text{Im}\left(\frac{\Gamma_{12}}{M_{12}}\right). \quad (27)$$

We discuss next the SM and new physics contributions to the coefficients C_i and $\tilde{C}_i$.

MFV contribution.—The SM W contribution is almost identical to that shown in Eq. (14) but for the fact that it is sufficient to keep only the top contribution (the $S_0(x_t)$ term) and changing the CKM factor to $(V_{tq}^*V_{tb})^2$. The new physics MFV charged-Higgs and chargino contributions are again identical to Eqs. (16) and (17), respectively, with the same change for the CKM factors. $C_1(m_t)$ is evolved down to m_b using Eq. (23).

Gluino contribution.—We only include the dominant gluino-right-handed-sbottom box diagrams with δ_{32}^{RL} and δ_{32}^{RR} mass insertions, since $\tilde{b}_R$ is the only relatively light down type squark in our scenario. These contributions are given by [6]

$$\tilde{C}_1^{\tilde{g}}(M_{\tilde{g}}) = ig_S^4[\Gamma_{b3}^{RR}(\Gamma_{q3}^{RR})^*]^2\left[\frac{1}{36}\tilde{I}_4 + \frac{1}{9}M_{\tilde{g}}^2 I_4\right],$$

$$\tilde{C}_2^{\tilde{g}}(M_{\tilde{g}}) = ig_S^4[\Gamma_{b3}^{RL}(\Gamma_{q3}^{RL})^*]^2\left[\frac{3}{2}M_{\tilde{g}}^2 I_4\right], \quad (28)$$

$$\tilde{C}_3^{\tilde{g}}(M_{\tilde{g}}) = -ig_S^4[\Gamma_{b3}^{RL}(\Gamma_{q3}^{RL})^*]^2\left[\frac{1}{2}M_{\tilde{g}}^2 I_4\right],$$

with the box integrals I_4 and $\tilde{I}_4$ given in Appendix B. The couplings are given by

$$\Gamma_{b3}^{RR} = \cos\theta_{32}^{RR}, \quad \Gamma_{b3}^{RL} = \cos\theta_{32}^{RL},$$
$$\Gamma_{d3}^{RR} = \sin\theta_{12}^{RR}\sin\theta_{32}^{RR}e^{-i(\gamma_{32}^{RR}+\gamma_{12}^{RR})},$$
$$\Gamma_{s3}^{RR} = -\cos\theta_{12}^{RR}\sin\theta_{32}^{RR}e^{-i\gamma_{32}^{RR}}, \quad (29)$$
$$\Gamma_{d3}^{RL} = \sin\theta_{12}^{RL}\sin\theta_{32}^{RL}e^{-i(\gamma_{32}^{RL}+\gamma_{12}^{RL})},$$
$$\Gamma_{s3}^{RL} = -\cos\theta_{12}^{RL}\sin\theta_{32}^{RL}e^{-i\gamma_{32}^{RL}},$$

obtained from the 3×3 mixing matrix that is the product of $C_{\tilde{d}_R\tilde{s}_R}$ and $C_{\tilde{b}_R\tilde{s}_R}$, with the mixing angles θ and phases γ given in Appendix A. In our U(2) model, if m_4 is of the

same order as A, based on the estimate in Eq. (8), we expect $\tilde{C}_1^{\tilde{g}}$ to receive the dominant gluino contribution from δ_{32}^{RR}. We will focus on this contribution in the following.

We point out in Appendix A, Eq. (A18), that $\tilde{d}_R\tilde{s}_R$ mixing can be generically large (near maximal), in which case the gluino contributions to both $B_d\bar{B}_d$ and $B_s\bar{B}_s$ mixing can be sizable. However, if $\epsilon'm_5^2 \ll \epsilon^2 m_2^2$, this mixing can be small and the gluino contribution to $B_d\bar{B}_d$ mixing is negligible since it is proportional to $\sin\theta_{12}^{RR}$ cf. Eqs. (28) and (29). The gluino contribution to $B_s\bar{B}_s$, however, can still be sizable in either case since it is proportional to $\cos\theta_{12}^{RR}$.

B. $B_d\bar{B}_d$ mixing

The $B_d\bar{B}_d$ mass difference (Δm_d), and CP violation in $B_d \to \psi K_s$ ($a_{\psi K_s}$) have been measured to be [10,17],

$$\Delta m_d = 0.502 \pm 0.007 \text{ ps}^{-1}, \qquad a_{\psi K_s} = 0.725 \pm 0.037. \quad (30)$$

In the SM, the usual notation is, $a_{\psi K_s}^{\text{SM}} \equiv \sin 2\beta$.

As we have already pointed out in Section III, the charged-Higgs and chargino MFV contributions add constructively with the SM contribution. The SM prediction agrees quite well with the data, but given the uncertainty in f_{B_d} cf. below Eq. (24), it might be possible to accommodate an MFV contribution up to a factor of about 1.3 bigger than the SM contribution. We show in Fig. 3 the region in MFV parameter space that satisfies this constraint, ignoring the gluino contribution.

As pointed out in the previous subsection, in general we expect in the U(2) model, $\tilde{d}_R\tilde{s}_R$ mixing to be near maximal, in which case the gluino contribution to $B_d\bar{B}_d$ can be sizable. The gluino contribution can then be important to both Δm_d and $a_{\psi K_s}$. Taking this into account, we can write $a_{\psi K_s} = \sin(2\beta + 2\theta_d)$, where θ_d is the new phase in $M_{12}(B_d)$ [18], and we have [10,19]

$$a_{\psi K_s} = \text{Im}(\lambda_{\psi K}), \qquad \lambda_{\psi K} \equiv -\frac{q}{p}\frac{\bar{A}(\bar{B}_d \to \psi K_s)}{A(B_d \to \psi K_s)},$$
$$\frac{q}{p} \equiv \sqrt{\frac{M_{12}^* - \frac{i}{2}\Gamma_{12}^*}{M_{12} - \frac{i}{2}\Gamma_{12}}}, \quad (31)$$

with M_{12} and Γ_{12} given in Eq. ((26)). (The "$-$" sign in $\lambda_{\psi K}$ is because the final state is CP odd.) In our case, $\Gamma_{12} \ll M_{12}$, so that

$$a_{\psi K_s} \approx \sin[\arg(M_{12})], \quad (32)$$

where "arg" denotes the argument of the complex quantity.

For the case when $\tilde{d}_R\tilde{s}_R$ mixing is large, we show the gluino contribution to $B_d\bar{B}_d$ in Fig. 4. The plot on the left also shows the constraint from $a_{\psi K_s}$, which is not shown in the plot on the right since almost the whole region shown is
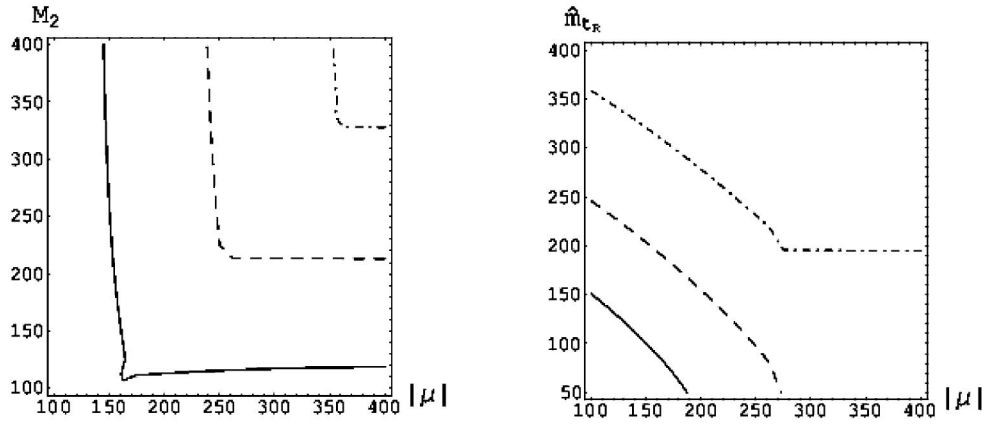
FIG. 3. The (dash-dot, dash, solid) curves are (1.1, 1.2, 1.3) contours of $|C_1^{\mathrm{MFV}}/C_1^{\mathrm{SM}}|$, showing the MFV contributions to $B_d\bar{B}_d$ mixing relative to the SM. Parameters not shown on a plot's axes are fixed as shown in Table I.

allowed. The region $[\pi < \arg(\delta_{32}^{RR}) < 2\pi]$ is not shown since it is identical to the region $(0, \pi)$. From the figure, we see that in the large mixing case, the constraint on δ_{32}^{RR} is quite strong. However, if $\tilde{d}_R\tilde{s}_R$ mixing is small, the constraint on δ_{32}^{RR} from $B_d\bar{B}_d$ mixing is weak.

C. $B_s\bar{B}_s$ mixing

$B_s\bar{B}_s$ mixing has not yet been observed and the current experimental limit is $\Delta m_{B_s} > 14.4$ ps^{-1} @ 95% C.L. [10]. The SM prediction is: 14ps$^{-1} < \Delta m_{B_s} < 20$ ps^{-1} [20]. The SM prediction for the dilepton asymmetry $A_{ll}^{B_s}$ is small, around 10^{-4} cf. references in Ref. [16].

$B_s\bar{B}_s$ mixing depends quite sensitively on δ_{32}^{RR}, and for the region in Fig. 4 allowed by $B_d\bar{B}_d$ mixing, we find $\Delta m_{B_s} \approx 22$ ps^{-1} and $A_{ll}^{B_s} \approx 5 \times 10^{-4}$. This Δm_{B_s} is a little higher than the SM prediction, although may be within the SM allowed range, given uncertainties.

As we pointed out in the previous subsection, if $\tilde{d}_R\tilde{s}_R$ mixing is small, then the $B_d\bar{B}_d$ mixing constraints

on δ_{32}^{RR} becomes weak. If such is the case, there are essentially no constraints from $B_d\bar{B}_d$ mixing, and we show contours of Δm_{B_s} and $A_{ll}^{B_s}$ in Fig. 5. We show only the range $[0 < \arg(\delta_{32}^{RR}) < \pi]$, since the $(\pi, 2\pi)$ range is identical to this. It can be seen that Δm_{B_s} can increase significantly above the SM prediction. The projected Run II sensitivity for Δm_{B_s} at the Tevatron with 2 fb^{-1} is around 40 ps^{-1} [20], and can probe a significant region of U(2) parameter space. If a higher value of Δm_{B_s} is measured than what the SM predicts, it would indicate the presence of new physics. Measuring $A_{ll}^{B_s}$ can also significantly constrain δ_{32}^{RR} as can be seen from Fig. 5 (right).

V. $\Delta B = 1$ FCNC PROCESSES

A. Effective Hamiltonian

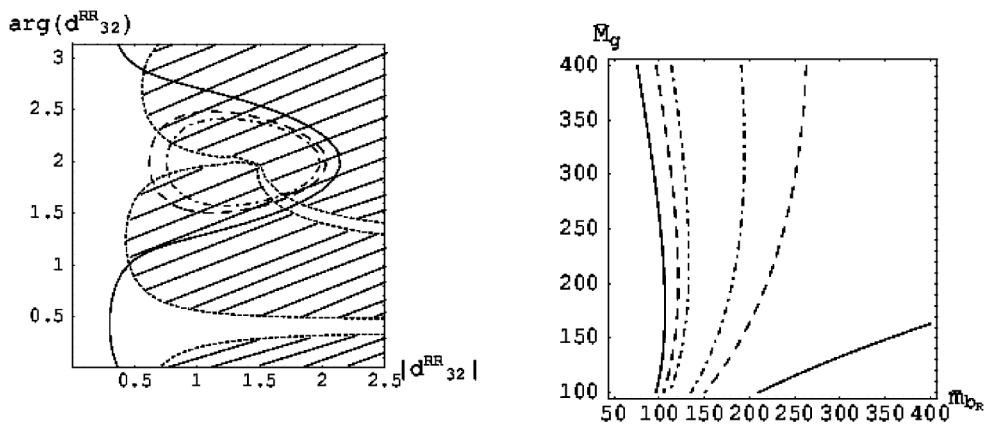The $\Delta B = 1$ effective Hamiltonian at a scale μ in the operator produce expansion (OPE) is [12,21,22]

FIG. 4. For large $\tilde{d}_R\tilde{s}_R$ mixing, the (dash-dot, dash, solid) curves are (0.9, 1.0, 1.25) contours of $|(C_1 + \tilde{C}_1)/C_1^{\mathrm{SM}}|$, showing the NMFV contributions to $B_d\bar{B}_d$ mixing relative to the SM. d_{32}^{RR} is defined in Eq. (7). The hatched region is excluded by $a_{\psi K_s}$. Parameters not shown on a plot's axes are fixed as shown in Table I.
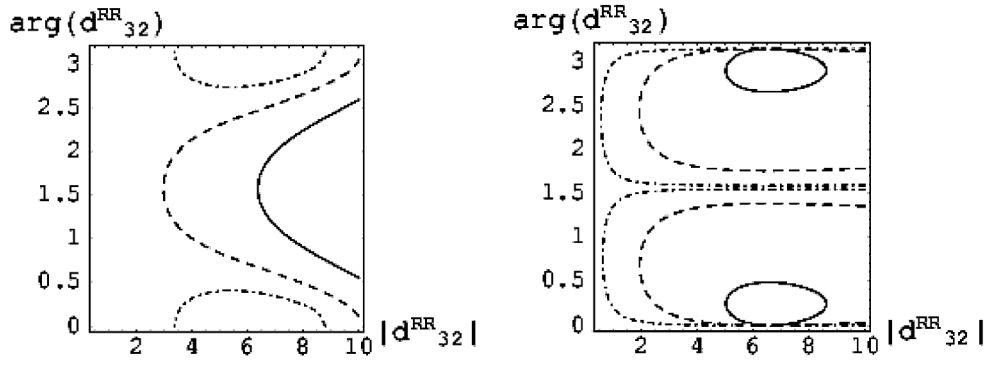
FIG. 5.   For small $\tilde{d}_R \tilde{s}_R$ mixing, the (dash-dot, dash, solid) curves are $(15, 25, 40 \text{ ps}^{-1})$ contours of Δm_{B_s} (left), and $(10^{-4}, 10^{-3}$ and $10^{-2})$ contours of $|A_{ll}^{B_s}|$ (right). d_{32}^{RR} is defined in Eq. (7). Parameters not shown on a plot's axes are fixed as shown in Table I.

$$\mathcal{H}_{\Delta B=1}^{\text{eff}} = -\frac{G_F}{\sqrt{2}} V_{ts} V_{tb}^* \left[\sum_{i=1\dots6,9,10} C_i(\mu)O_i(\mu) + C_{7\gamma}(\mu)O_{7\gamma}(\mu) + C_{8g}(\mu)O_{8g}(\mu) \right], \tag{33}$$

with

$$O_1 = (\bar{s}_\alpha c_\beta)_{V-A}(\bar{c}_\beta b_\alpha)_{V-A}, \qquad O_2 = (\bar{s}c)_{V-A}(\bar{c}b)_{V-A}, \qquad O_3 = (\bar{s}b)_{V-A}\sum_q(\bar{q}q)_{V-A},$$

$$O_4 = (\bar{s}_\alpha b_\beta)_{V-A}\sum_q(\bar{q}_\beta q_\alpha)_{V-A}, \qquad O_5 = (\bar{s}b)_{V-A}\sum_q(\bar{q}q)_{V+A}, \qquad O_6 = (\bar{s}_\alpha b_\beta)_{V-A}\sum_q(\bar{q}_\beta q_\alpha)_{V+A},$$

$$O_{7\gamma} = \frac{e}{8\pi^2}m_b\bar{s}_\alpha\sigma^{\mu\nu}(1+\gamma_5)b_\alpha F_{\mu\nu}, \qquad O_{8g} = \frac{g_s}{8\pi^2}m_b\bar{s}_\alpha\sigma^{\mu\nu}(1+\gamma_5)T^a_{\alpha\beta}b_\beta G^a_{\mu\nu}, \qquad O_9 = (\bar{s}b)_{V-A}(\bar{e}e)_V, \tag{34}$$

$$O_{10} = (\bar{s}b)_{V-A}(\bar{e}e)_A,$$

where, the subscript $(V \pm A)$ means $\gamma_\mu(1 \pm \gamma_5)$, and $F^{\mu\nu}$, $G^{\mu\nu}$ are the electromagnetic and color field strengths, respectively.

The Wilson coefficients can be computed at the scale M_W (the W boson mass), and then run down to the scale m_b (the b quark mass). Below, when no scale is specified for the coefficients, it is understood to be at m_b, i.e., $C_i \equiv C_i(m_b)$. The coefficients when run down from M_W to m_b mix under renormalization, so that [23][5]

$$C_j = \sum_{i=1}^8 k_{ji}\eta^{a_i}, \qquad (j = 1, \dots, 6),$$

$$C_{7\gamma} = \eta^{16/23}C_{7\gamma}(M_W) + \frac{8}{3}(\eta^{14/23} - \eta^{16/23})C_{8g}(M_W)$$

$$+ \sum_{i=1}^8 h_i\eta^{a_i}C_2(M_W),$$

$$C_{8g} = \eta^{14/23}C_{8g}(M_W) + \sum_{i=1}^8 \bar{h}_i\eta^{a_i}C_2(M_W), \tag{35}$$

where $\eta \equiv \alpha_s(M_W)/\alpha_s(m_b) \approx 0.56$ and h_i, $\bar{h}_i$, a_i and k_{ji}

are given in Ref. [12]. In addition, the evolution equation for C_9 is given in Ref. [22], and C_{10} is not renormalized.

Separating out the new physics contribution to the renormalization group evolution, i.e., Eq. (35), we get

$$C_2 = C_2^{\text{SM}},$$

$$C_{7\gamma} = C_{7\gamma}^{\text{SM}} + 0.67C_{7\gamma}^{\text{new}}(M_W) + 0.09C_{8g}^{\text{new}}(M_W), \tag{36}$$

$$C_{8g} = C_{8g}^{\text{SM}} + 0.70C_{8g}^{\text{new}}(M_W),$$

in which the superscript "SM" indicates the contribution from the SM, and "new" from new physics.

SM contribution.—The SM $W^\pm$ contribution to $C_{7\gamma}(M_W)$ and $C_{8g}(M_W)$ are given by [25,26]

$$C_2^{\text{SM}}(M_W) = 1, \tag{37}$$

$$C_{7\gamma,8g}^{\text{SM}}(M_W) = \frac{3}{2}F_{7,8}^{LL}\left(\frac{m_t^2}{M_W^2}\right), \tag{38}$$

where $F_{7,8}^{LL}(x)$ are given in Appendix B. Using Eq. (35) we can compute C_2^{SM}, $C_{7\gamma}^{\text{SM}}$ and C_{8g}^{SM}.

In the following, we will discuss, in order, the new physics contribution arising from the charged-Higgs boson ($H^\pm$), charginos ($\tilde{\chi}^\pm$) and gluinos ($\tilde{g}$).

---

[5]Here, as a first step, we use the leading order result. The next to leading order result can be found in Ref. [24].

Charged-Higgs ($H^{\pm}$) *contribution.*—The charged-Higgs contribution to $B_d \to X_s \gamma$ is given by [5,26,27]

$$C^{H}_{7\gamma,8g}(M_W) = \frac{1}{2}\cot^2\beta F^{LL}_{7,8}\left(\frac{m_t^2}{M_H^2}\right) + \tilde{F}^{LL}_{7,8}\left(\frac{m_t^2}{M_H^2}\right), \quad (39)$$

where $F^{LL}_{7,8}(x)$ and $\tilde{F}^{LL}_{7,8}(x)$ are given in Appendix B.

Chargino ($\tilde{\chi}^{\pm}$) *contribution.*—The chargino-stop contribution can be comparable to the SM contribution for a light stop and chargino. In the scenario that we are considering, the stop mixing angle is negligibly small and $m_{\tilde{t}_L} \approx m_{\tilde{t}_1} \sim \tilde{m}_0$ and $m_{\tilde{t}_R} \approx m_{\tilde{t}_2} \sim M_W$. We therefore run the $\tilde{t}_1$ contribution from $\tilde{m}_0$ down to M_W and evaluate the $\tilde{t}_2$ contribution at M_W. The chargino-stop contribution is [5,26,27]

$$C^{\tilde{\chi}\tilde{t}_1}_{7\gamma,8g}(\tilde{m}_0) = -\sum_{j=1}^{2}\left[|\Gamma_L^{1j}|^2\frac{M_W^2}{m_{\tilde{t}_1}^2}F^{LL}_{7,8}\left(\frac{m_{\tilde{t}_1}^2}{M_{\tilde{\chi}_j}^2}\right) + \gamma_{RL}^{1j}\frac{M_W}{M_{\tilde{\chi}_j}}F^{RL}_{7,8}\left(\frac{m_{\tilde{t}_1}^2}{M_{\tilde{\chi}_j}^2}\right)\right],$$

$$(40)$$

$$C^{\tilde{\chi}\tilde{t}_2}_{7\gamma,8g}(M_W) = -\sum_{j=1}^{2}\left[|\Gamma_L^{2j}|^2\frac{M_W^2}{m_{\tilde{t}_2}^2}F^{LL}_{7,8}\left(\frac{m_{\tilde{t}_2}^2}{M_{\tilde{\chi}_j}^2}\right) + \gamma_{RL}^{2j}\frac{M_W}{M_{\tilde{\chi}_j}}F^{RL}_{7,8}\left(\frac{m_{\tilde{t}_2}^2}{M_{\tilde{\chi}_j}^2}\right)\right],$$

where the loop functions $F^{RL}_{7,8}$ are given in Appendix B, and Γ_L^{ij} and γ_{RL}^{ij} contain the stop and chargino mixing matrices. Explicit expressions for Γ_L^{ij}, γ_{RL}^{ij} and the renormalization group equations to evolve $C^{\tilde{\chi}\tilde{t}_1}_{7\gamma,8g}(\tilde{m}_0)$ down to M_W are given in Ref. [26].

Gluino ($\tilde{g}$) *contribution.*—In our NMFV scenario, the gluino contributions can be sizable since they couple with strong interaction strength. Furthermore, because the sbottom mixing angle is negligibly small, $m_{\tilde{b}_L} \approx m_{\tilde{b}_1} \sim \tilde{m}_0$ and $m_{\tilde{b}_R} \approx m_{\tilde{b}_2} \sim M_W$. Keeping only the $M_{\tilde{g}}/m_b$ enhanced piece, the gluino contribution is [5]

$$C^{\tilde{g}}_{7\gamma}(M_W) = -\frac{4\pi\alpha_s\sqrt{2}}{G_F V_{ts}^* V_{tb}}\frac{M_{\tilde{g}}}{m_b}\cos\theta_{32}^{RL}\sin\theta_{32}^{RL}e^{-i\gamma_{32}^{RL}}\frac{1}{9}\left[\frac{1}{m_{\tilde{b}_2}^2}F_4\left(\frac{M_{\tilde{g}}^2}{m_{\tilde{b}_2}^2}\right) - \frac{1}{m_{\tilde{b}_1}^2}F_4\left(\frac{M_{\tilde{g}}^2}{m_{\tilde{b}_1}^2}\right)\right],$$

$$(41)$$

$$C^{\tilde{g}}_{8g}(M_W) = \frac{4\pi\alpha_s\sqrt{2}}{G_F V_{ts}^* V_{tb}}\frac{M_{\tilde{g}}}{m_b}\cos\theta_{32}^{RL}\sin\theta_{32}^{RL}e^{-i\gamma_{32}^{RL}}\frac{1}{8}\left[\frac{1}{m_{\tilde{b}_2}^2}F_{\tilde{g}}\left(\frac{M_{\tilde{g}}^2}{m_{\tilde{b}_2}^2}\right) - \frac{1}{m_{\tilde{b}_1}^2}F_{\tilde{g}}\left(\frac{M_{\tilde{g}}^2}{m_{\tilde{b}_1}^2}\right)\right],$$

where the mixing angle θ_{32}^{RL} and phase γ_{32}^{RL} are defined in Appendix A, and F_4 and $F_{\tilde{g}}$ are defined in Appendix B. In the above equation, we have neglected the effect of running the $\tilde{b}_1$ contribution from $\tilde{m}_0$ to M_W as the $\tilde{b}_2$ contribution is dominant.

The dominant new physics contribution is given by adding Eqs. (39)–(41), which yields

$$C^{\text{new}}_{7\gamma,8g}(M_W) = C^H_{7\gamma,8g}(M_W) + C^{\tilde{\chi}}_{7\gamma,8g}(M_W) + C^{\tilde{g}}_{7\gamma,8g}(M_W).$$

$$(42)$$

In what follows we will discuss in detail the new physics contribution predicted by the U(2) model to the rare decay processes $B_d \to X_s\gamma$, $B_d \to X_sg$, $B_d \to X_s\ell^+\ell^-$ and $B_d \to \phi K_s$.

B. $B_d \to X_s\gamma$, $B_d \to X_sg$

The dominant operators contributing to $B_d \to X_s\gamma$ and $B_d \to X_sg$ are O_2, $O_{7\gamma}$ and O_{8g}. The decay branching ratio B.R.$(B_d \to X_s\gamma)$, at leading order, normalized to the semileptonic B.R.$(B_d \to X_c e\bar{\nu}) \approx 10.5\%$, is given by [23,28,29]

$$\frac{\Gamma(B_d \to X_s\gamma)}{\Gamma(B_d \to X_c e\bar{\nu})}\bigg|_{[E_\gamma > (1-\delta)E_\gamma^{\max}]} = \frac{6\alpha}{\pi}\frac{1}{g(\frac{m_c}{m_b})}\left|\frac{V_{ts}^* V_{tb}}{V_{cb}}\right|^2|C_{7\gamma}|^2,$$

$$(43)$$

where $g(z) \equiv 1 - 8z^2 + 8z^6 - z^8 - 24z^4\ln(z)$ is a phase space function, and δ is the fractional energy cut, i.e., only photon energy $E_\gamma > (1-\delta)E_\gamma^{\max}$ is accepted.

The CP asymmetry in $B_d \to X_s\gamma$ is given by [29]

$$A^{B_d \to X_s\gamma}_{\text{CP}}(\delta) = \frac{\Gamma(\bar{B}_d \to X_s\gamma) - \Gamma(B_d \to X_{\bar{s}}\gamma)}{\Gamma(\bar{B}_d \to X_s\gamma) + \Gamma(B_d \to X_{\bar{s}}\gamma)}\bigg|_{E_\gamma > (1-\delta)E_\gamma^{\max}},$$

$$= \frac{1}{|C_{7\gamma}|^2}\{a_{27}(\delta)\text{Im}[C_2 C_{7\gamma}^*]$$

$$+ a_{87}(\delta)\text{Im}[C_{8g}C_{7\gamma}^*] + a_{28}(\delta)\text{Im}[C_2 C_{8g}^*]\}.$$

$$(44)$$

For $\delta = 0.15$, which is a typical experimental cut, we use $a_{27} = 0.0124$, $a_{87} = -0.0952$ and $a_{28} = 0.0004$ [29].

The experimentally measured [17] branching ratio is B.R.$(B_d \to X_s\gamma) = (3.52^{+0.3}_{-0.28}) \times 10^{-4}$. In the SM, we have $C_2^{\text{SM}} \approx 1.11$, $C_{7\gamma}^{\text{SM}} \approx -0.31$ and $C_{8g}^{\text{SM}} \approx -0.15$. The SM prediction for B.R.$(B_d \to X_s\gamma)$, which depends on $|C_{7\gamma}|$ cf. Eq. (43), is largely consistent with experiment,

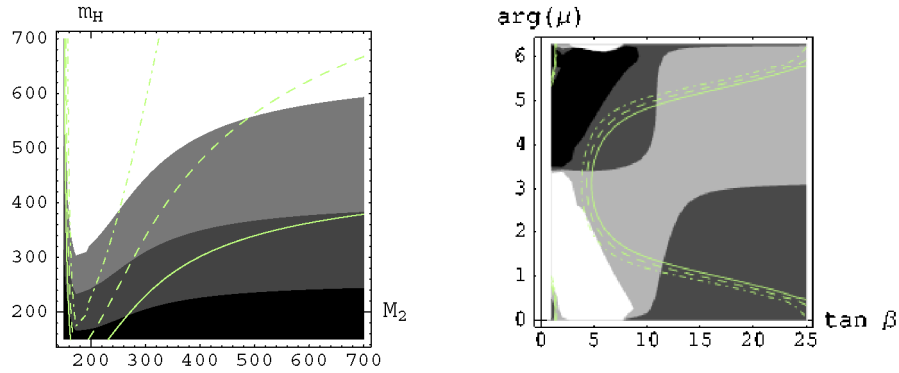FIG. 6 (color online). The boundaries between the shaded regions show (2.5%, 3% ,3.5%) (darkest to lightest) contours of $A_{\mathrm{CP}}^{B_d \to X_s \gamma}$ as a function of m_H and M_2 (left), and, (-3.5%, 0%, 3.5%) (darkest to lightest) contours of $A_{\mathrm{CP}}^{B_d \to X_s \gamma}$ as a function of $\tan\beta$ and $\arg(\mu)$ (right). Superimposed is the experimental 2σ allowed contours of B.R.$(B_d \to X_s \gamma)$. Parameters not shown on a plot's axes are fixed as shown in Table I.

and new physics contributions to $|C_{7\gamma}|$ is constrained by this branching ratio. In the context of SUSY this has been analyzed, for example, in Refs. [5,23,30].

The SM CP asymmetry in $B_d \to X_s \gamma$ is of the order of 1%, so that a larger CP asymmetry measured would imply new physics [29]. The present limit at 95% C.L. is [17,31,32] $-0.07 < A_{\mathrm{CP}}^{B_d \to X_s \gamma} < 0.07$.

The B.R.$(B_d \to X_s g)$ is obtained simply from Eq. (43)

$$\frac{\Gamma(B_d \to X_s g)}{\Gamma(B_d \to X_c e \bar{\nu})} = C(R) \frac{6\alpha_s}{\pi} \frac{1}{g(\frac{m_c}{m_b})} \left| \frac{V_{ts}^* V_{tb}}{V_{cb}} \right|^2 |C_{8g}|^2, \tag{45}$$

where the SU(3) quadratic Casimir $C(R) = 4/3$. The B.R.$(B_d \to X_s g)$ has large experimental and theoretical uncertainties and Ref. [33] suggests that the data might prefer a B.R. value of around 10%.

Figures 6 and 7 show the interplay between the $W^{\pm}$, $H^{\pm}$, $\tilde{\chi}^{\pm}$ and $\tilde{g}$ contributions to $B_d \to X_s \gamma$, where the sum of these contributions to the magnitude of $C_{7\gamma}$ is constrained by B.R.$(B_d \to X_s \gamma)$. The experimental data on $B_d \to X_s \gamma$ allows (at 2σ) the region bounded by the contours shown in the figures. In the plots, the parameters are as given in

Table I, and some relevant ones are varied as shown in the figures.

To illustrate the dependence on the MFV parameters, we consider, for example, in Fig. 6, the dependence of $A_{\mathrm{CP}}^{B_d \to X_s \gamma}$ and B.R.$(B_d \to X_s \gamma)$ as a function of m_H and M_2 (left) and as a function of $\tan\beta$ and $\arg(\mu)$ (right), for the choice of parameters shown in Table I. The experimental 2σ allowed contours of B.R.$(B_d \to X_s \gamma)$ are also shown. In Fig. 7 (left), the shaded regions show $A_{\mathrm{CP}}^{B_d \to X_s \gamma}$ as a function of the magnitude and argument of d_{32}^{RL}, the dimensionless $\mathcal{O}(1)$ coefficient defined in Eq. (8). In Fig. 7 (right), we show contours of B.R.$(B_d \to X_s g)$, and a B.R. of up to about 15% can be accommodated in this model.

C. $B_d \to X_s \ell^+ \ell^-$

The dominant operators contributing to $B_d \to X_s \ell^+ \ell^-$ ($\ell = e, \mu$) are $O_{7\gamma}$, O_9 and O_{10}. It is usual to define

$$C_9(\mu) \equiv \frac{\alpha}{2\pi} \tilde{C}_9(\mu), \qquad C_{10} \equiv \frac{\alpha}{2\pi} \tilde{C}_{10},$$
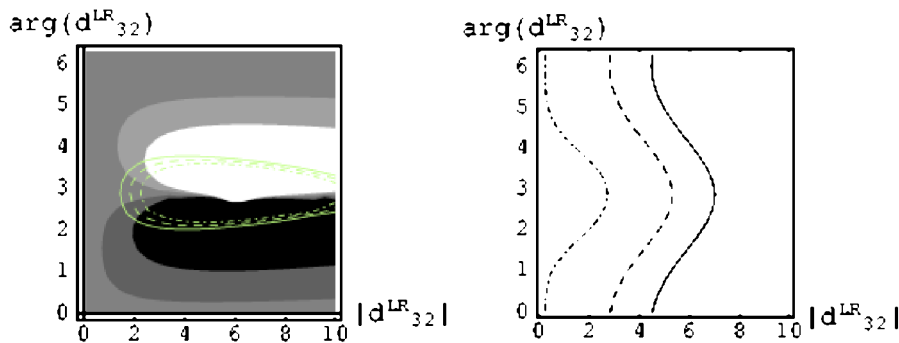
and

FIG. 7 (color online). The boundaries between the shaded regions show (-7%, -3%, 3%, 7%) (darkest to lightest) contours of $A_{\mathrm{CP}}^{B_d \to X_s \gamma}$ (left) with experimentally allowed 2σ contours of B.R.$(B_d \to X_s \gamma)$ superimposed, and, 1%, 7.5% and 15% contours of predicted B.R.$(B_d \to X_s g)$ (right). Parameters not shown on a plot's axes are fixed as shown in Table I.

TABLE II. The current data for $B_d \to X_s \ell^+ \ell^-$.

	Experiment [17]	SM prediction
B.R.$(B_d \to X_s \ell^+ \ell^-)$	$4.46^{+0.98}_{-0.96} \times 10^{-6}$	5.3×10^{-6}

$$\hat{s} \equiv \frac{(p_{\ell^+} + p_{\ell^-})^2}{m_b^2}. \tag{46}$$

The (differential) partial width $\frac{d}{d\hat{s}}\Gamma(B_d \to X_s \ell^+ \ell^-)$, normalized to $\Gamma(B_d \to X_c e \bar{\nu})$, is given by [22]:

$$R(\hat{s}) \equiv \frac{\frac{d}{d\hat{s}}\Gamma(B_d \to X_s \ell^+ \ell^- B_d \to X_s \ell^+ \ell^-)}{\Gamma(B_d \to X_c e \bar{\nu} B \to X_c e \bar{\nu})}$$

$$= \frac{\alpha^2}{4\pi^2}\left|\frac{V_{ts}^* V_{tb}}{V_{cb}}\right|^2 \frac{(1-\hat{s})^2}{f(\frac{m_c}{m_b})\kappa(\frac{m_c}{m_b})}\left[(1+2\hat{s})(|\tilde{C}_9^{\mathrm{eff}}|^2\right.$$

$$\left. + |\tilde{C}_{10}|^2) + 4\left(1 + \frac{2}{\hat{s}}\right)|C_{7\gamma}|^2 + 12\mathrm{Re}(C_{7\gamma}\tilde{C}_9^{\mathrm{eff}})\right], \tag{47}$$

where f and κ are phase space functions and $\tilde{C}_9^{\mathrm{eff}}$ is the QCD corrected $\tilde{C}_9$, given in terms of $\tilde{C}_9$ and C_i ($i = 1 \ldots 6$) [22]. Integrating this we get the prediction for the decay branching ratios and we show this in Table II for the SM along with the experimental result [17]. We choose the lower limit on the integration to correspond to a typical experimental choice, $(p_{\ell^+} + p_{\ell^-})^2 > (0.2 \text{ GeV})^2$. Since the rate of $B_d \to X_s \ell^+ \ell^-$ is down by the square of the electromagnetic coupling constant compared to $B_d \to X_s \gamma$, the experimental errors are comparatively larger.

Figure 8 shows the contours of B.R.$(B_d \to X_s \ell^+ \ell^-)$ as a function of d_{32}^{RL}. Compared to B.R.$(B_d \to X_s \gamma)$ cf. Figure 7 (left), the $B_d \to X_s \ell^+ \ell^-$ constraint is not very stringent right now, and improved statistics at the B-factories could place tighter constraints on the parameter space.
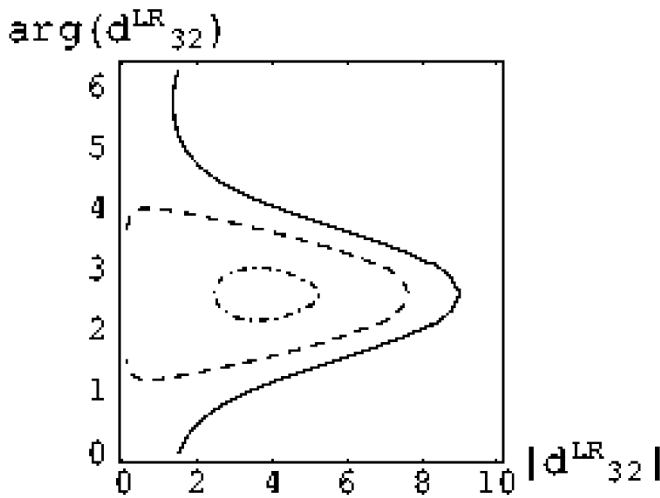

FIG. 8. The (dash-dot, dash, solid) curves are $(5.25, 6.25, 7.25) \times 10^{-6}$ contours of $B_d \to X_s \ell^+ \ell^-$. Parameters not shown on the plot's axes are fixed as shown in Table I.

TABLE III. The current data for $B_d \to \phi K_s$.

	Experiment [17]	SM prediction
B.R.$(B_d \to \phi K_s)$	$8.3^{+1.2}_{-1.0} \times 10^{-6}$	$\sim 5 \times 10^{-6}$
$S_{\phi K}$	0.34 ± 0.2	0.725 ± 0.037
$C_{\phi K}$	-0.04 ± 0.17	0

D. $B_d \to \phi K_s$

The decay $B_d \to \phi K_s$ ($b \to s s \bar{s}$ at the quark level) can be a sensitive probe of new physics since the leading order SM contribution is one-loop suppressed, and loop processes involving heavy SUSY particles can contribute significantly. However, the computation of B.R.$(B_d \to \phi K_s)$ suffers from significant theoretical uncertainties in calculating the hadronic matrix elements. We follow the factorization approach, details of which are presented in Ref. [34]. The theoretical uncertainties largely cancel in the CP asymmetry, and is therefore a good probe of new physics.

The CP asymmetry in $B_d \to \phi K_s$ is defined by

$$A_{\mathrm{CP}}^{B_d \to \phi K_s} \equiv \frac{\Gamma[\bar{B}_d(t) \to \phi K_s] - \Gamma[B_d(t) \to \phi K_s]}{\Gamma[\bar{B}_d(t) \to \phi K_s] + \Gamma[B_d(t) \to \phi K_s]} \tag{48}$$

$$= -C_{\phi K}\cos(\Delta m_{B_d} t) + S_{\phi K}\sin(\Delta m_{B_d} t), \tag{49}$$

where

$$C_{\phi K} \equiv \frac{1 - |\lambda_{\phi K}|^2}{1 + |\lambda_{\phi K}|^2}, \qquad S_{\phi K} \equiv \frac{2\mathrm{Im}(\lambda_{\phi K})}{1 + |\lambda_{\phi K}|^2},$$

$$\lambda_{\phi K} \equiv -e^{-2i(\beta + \theta_d)}\frac{\bar{A}(B_d \to \phi K_s)}{A(\bar{B}_d \to \phi K_s)},$$

where $B_d(t)$ represents the state that is a B_d at time $t = 0$, Δm_{B_d} is the $B_d \bar{B}_d$ mass difference, β is the usual angle in the SM CKM unitarity triangle fits to the CP asymmetry in $B_d \to J/\psi K_s$, and θ_d is any new physics contributions to $B_d \bar{B}_d$ mixing (θ_d is discussed in Section IV B). The SM predicts that the CP asymmetry in $B_d \to \phi K_s$ and $B_d \to J/\psi K_s$ should be the same, i.e., $S_{\phi K} = \sin 2\beta$.

The $\bar{B}_d \to \phi K_s$ amplitude and partial decay width are given by [8,34]:

$$A(\bar{B}_d \to \phi K_s) = \sum_{p=u,c}\lambda_p\left[(a_3 + a_4^p + a_5)\right.$$

$$\left. - \frac{1}{2}(a_7 + a_9 + a_{10}^p)\right] \tag{50}$$

$$\Gamma(\bar{B}_d \to \phi K_s) = \frac{G_F^2 f_\phi^2 m_B^3}{32\pi}(F_1^{B \to K})^2 |A(\bar{B}_d \to \phi K_s)|^2$$

$$\times \left[\lambda\left(1, \frac{m_\phi^2}{m_B^2}, \frac{m_K^2}{m_B^2}\right)\right]^{3/2} \tag{51}$$

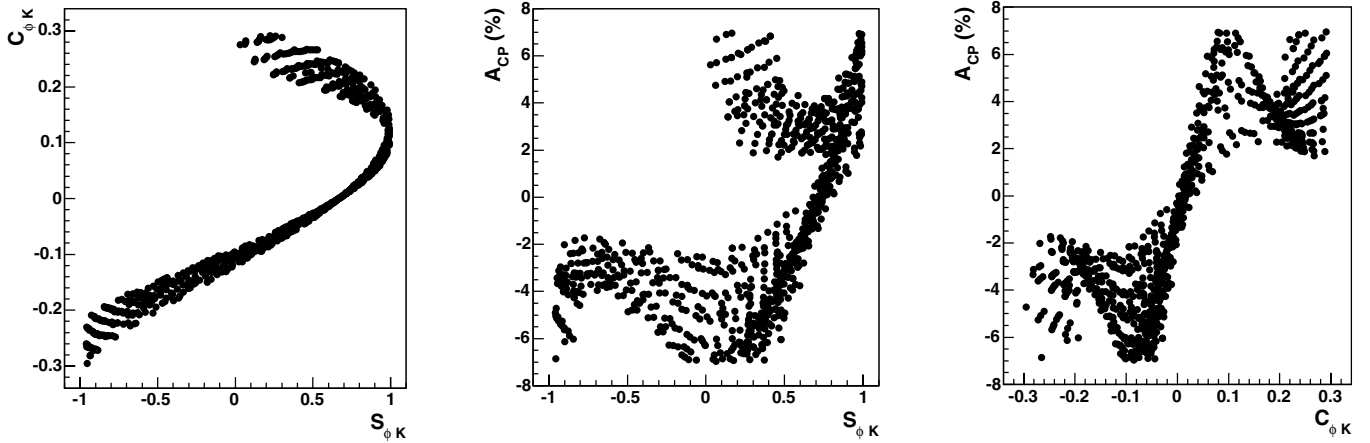FIG. 9. $A_{CP}^{B_d \to X_s \gamma}$, $S_{\phi K}$ and $C_{\phi K}$ for points that satisfy all experimental constraints (within 2σ), resulting from a scan over d_{32}^{LR} and $\arg(\mu)$, for small $\tilde{d}_R \tilde{s}_R$ mixing (negligible θ_d). All other parameters are fixed as shown in Table I.
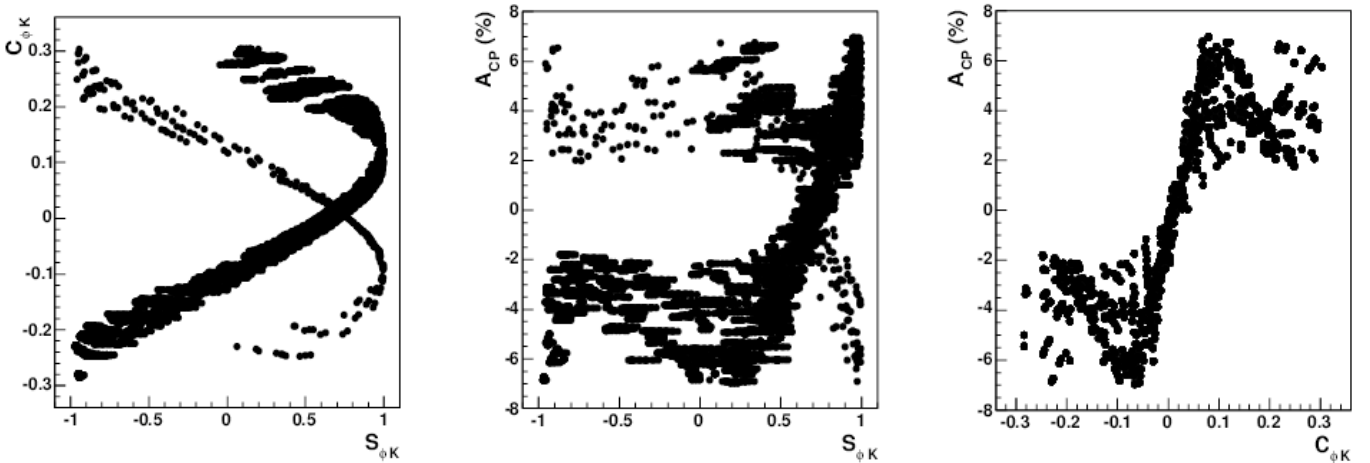

FIG. 10. $A_{CP}^{B_d \to X_s \gamma}$, $S_{\phi K}$ and $C_{\phi K}$ for points that satisfy all experimental constraints (within 2σ), resulting from a scan over $d_{32}^{LR,RR}$ and $\arg(\mu)$, for large $\tilde{d}_R \tilde{s}_R$ mixing (nonzero θ_d). All other parameters are fixed as shown in Table I.

where the phase space function[6] $\lambda(x, y, z) \equiv x^2 + y^2 + z^2 - 2xy - 2yz - 2zx$, the ϕ decay constant $f_\phi = 237$ MeV, the form factor $F_1^{B \to K} = 0.38$ and $\lambda_p \equiv V_{pb} V_{ps}^*$. The SM a_i's, in terms of the C_i's, are given in Ref. [34] to which we add the new physics contribution given in Eq. (42). We do not include the power-suppressed weak annihilation operators and we refer the reader to Refs. [34,35] for a more complete discussion. As explained in Section II B, we are only including the δ_{32}^{RL} SUSY contribution, as this is the dominant one. The amplitude for the CP conjugate process $B_d \to \phi K_s$ is obtained by taking $\lambda_p \to \lambda_p^*$.

The current $B_d \to \phi K_s$ experimental average [17] is summarized in Table III. The SM requires $S_{\phi K} = S_{J/\psi K} \equiv$ sin2β, but the experimental data has about a 2σ discrepancy between $S_{\phi K}$ and $S_{J/\psi K}$.[7] Though not convincing yet, this could be an indication of new physics and we ask if this can be naturally explained in the theory we are considering.

We showed in Section IV B, that if $\tilde{d}_R \tilde{s}_R$ mixing is small, there is no significant new phase in $M_{12}(B_d)$ (i.e., $\theta_d \approx 0$). For this case, we scan the parameter space $\arg(\mu)$, $|\delta_{32}^{RL}|$, $\arg(\delta_{32}^{RL})$, and in Fig. 9 show a scatter-plot of the points that satisfy all experimental constraints including B.R.($B_d \to X_s \gamma$) and B.R.($B_d \to \phi K_s$). We find that it is possible to satisfy all experimental constraints including the recent $B_d \to \phi K_s$ data shown in Table III in the framework we

---

[6]We thank Liantao Wang for clarifying the expression for $\lambda(x, y, z)$.

[7]The significance of the discrepancy between $S_{b \to s}$ and $S_{b \to c}$ is bigger, currently at about 3.5σ, where $S_{b \to s}$ and $S_{b \to c}$ are the averages over all measured $b \to s$ (penguin) and $b \to c$ modes, respectively.

are considering. Furthermore, there are strong correlations between $A_{\rm CP}^{B_d \to X_s \gamma}$, $S_{\phi K}$, and $C_{\phi K}$. As the accuracy of the experimental data improve, we can use these correlations to (in)validate the choices that we make in our model.

Large $\tilde{d}_R \tilde{s}_R$ mixing can lead to a nonzero θ_d which depends on $|\delta_{32}^{RR}|$ as explained in Section IV B. We therefore include this new phase and perform a scan over $|\delta_{32}^{RR}|$, $\arg(\delta_{32}^{RR})$, $\arg(\mu)$, $|\delta_{32}^{RL}|$ and $\arg(\delta_{32}^{RL})$. We show the points that satisfy all experimental constraints and the resulting $A_{\rm CP}^{B_d \to X_s \gamma}$, $S_{\phi K}$, and $C_{\phi K}$ in Fig. 10. We again see from Fig. 10 that $A_{\rm CP}^{B_d \to X_s \gamma}$, $S_{\phi K}$, and $C_{\phi K}$ are strongly correlated, although the effect of the new phase in $B_d \bar{B}_d$ mixing allows new regions of parameter space compared to the small mixing case shown in Fig. 9. Even in the case of large mixing we find that it is possible to satisfy all experimental data including the $S_{\phi K}$ and $C_{\phi K}$. One feature that we find in either large or small mixing case is that sign $(C_{\phi K})$ is positively correlated with sign $(A_{\rm CP}^{B_d \to X_s \gamma})$. Thus, further data could shed light on the validity of the choices that we make in our model.

VI. CONCLUSIONS

A supersymmetric U(2) theory has the potential to explain the gauge hierarchy and flavor problems in the SM. We assumed an effective SUSY mass spectrum just above the weak scale, the only relatively light scalars being the right-handed-stop and sbottom (weak scale masses). We analyzed what such a hypothesis would imply for K and B meson observables by including all the dominant contributions that can interfere in a certain observable. Although for definiteness we considered a U(2) framework, our conclusions hold for any theory with a similar SUSY mass spectrum and structure of the squark mass matrix.

The CP violation parameter in Kaon mixing, ϵ_K, can impose constraints on the MFV parameter space of our model, as we showed in Fig. 2, while the gluino contribution to ϵ_K is negligible. There is sufficient room to accommodate the MFV contributions to ϵ_K, given the present uncertainty in the lattice computation of the Bag parameter B_K.

We find that $B_d \bar{B}_d$ mixing and $a_{\psi K_s}$ ($\sin 2\beta$) can impose constraints on the supersymmetric U(2) theory. In addition to the MFV contribution, if $\tilde{d}_R \tilde{s}_R$ mixing is large, the gluino contributions to $B_d \bar{B}_d$ mixing can be significant leading to a strong constraint on the 32 entry of the RR squark mass matrix, δ_{32}^{RR}, as shown in Fig. 4. Furthermore, in this case, there is a new phase in the $B_d \bar{B}_d$ mixing amplitude coming from the SUSY sector. However, if $\tilde{d}_R \tilde{s}_R$ mixing is small, the constraint on δ_{32}^{RR} from $B_d \bar{B}_d$ mixing is weak.

$B_s \bar{B}_s$ mixing most sensitively depends on δ_{32}^{RR} in the SUSY U(2) theory. If δ_{32}^{RR} is unconstrained by $B_d \bar{B}_d$ mixing (small $\tilde{d}_R \tilde{s}_R$ mixing), we showed that Δm_{B_s} can be increased to quite large values (up to about 40 ps^{-1}) cf. Fig. 5 . The current and upcoming experiments can reach

sensitivities required to see the SM prediction for Δm_{B_s}. Seeing a higher value, or not seeing a signal at all, might hint at some new physics of the type we are considering. We also presented expectations for the B_s dilepton asymmetry, $A_{ll}^{B_s}$, which can constrain δ_{32}^{RR}.

The experimental data on B.R.$(B_d \to X_s \gamma)$ imposes a constraint on the SUSY theory. While satisfying this constraint, we showed that an enhancement in CP Violation in $B_d \to X_s \gamma$ is possible. Since in the SM, $A_{\rm CP}^{B_d \to X_s \gamma}$ is predicted to be less than 1%, if a much larger value is measured, it would clearly point to new physics. In Fig. 7 we presented the expectations for $A_{\rm CP}^{B_d \to X_s \gamma}$ and B.R.$(B_d \to X_s g)$ while varying the magnitude and phase of δ_{32}^{RL}. We also presented expectations for B.R.$(B_d \to X_s \ell^+ \ell^-)$ in Fig. 8.

The present experimental data on the CP violation in $B_d \to \phi K_s$ has about a 2σ deviation from the SM prediction, and it will be very interesting to see if this would persist with more data. We showed that such a deviation can be accommodated in the framework we are considering, both for large or small $\tilde{d}_R \tilde{s}_R$ mixing. We showed, in Fig. 10, that $A_{\rm CP}^{B_d \to X_s \gamma}$ can be enhanced significantly while satisfying all other experimental bounds including the present data on $S_{\phi K}$ and $C_{\phi K}$. In Figs. 9 and 10 , for small and large $\tilde{d}_R \tilde{s}_R$ mixing, respectively, we see strong correlations between $A_{\rm CP}^{B_d \to X_s \gamma}$, $S_{\phi K}$, and $C_{\phi K}$. Comparing these with upcoming data with improved precision could shed light on the validity of the choices that we make in our model.

We conclude by remarking that the prospects are exciting for discovering SUSY in B-meson processes at current and upcoming colliders. Here, we showed this for a SUSY U(2) model. To unambiguously establish that it is a SUSY U(2) theory, and to determine the various SUSY breaking parameters, will require looking at a broad range of observables.

APPENDIX A: MIXING ANGLES

The charged SU(2) Majorana gauginos $\tilde{W}_1$, $\tilde{W}_2$ can be combined to form the Dirac spinor

$$\tilde{W}^+ = \frac{1}{\sqrt{2}} \begin{pmatrix} \tilde{W}_\alpha^+ \\ \tilde{W}^{-\dot{\alpha}} \end{pmatrix}, \tag{A1}$$

where $\tilde{W}_\alpha^\pm = \tilde{W}_{1\alpha} \pm i\tilde{W}_{2\alpha}$. The up and down type Higgsinos can be combined to form the Dirac spinor

$$\tilde{H}^+ = \begin{pmatrix} \tilde{H}_{u\alpha} \\ \tilde{H}_d^{\dot{\alpha}} \end{pmatrix}. \tag{A2}$$

The chargino mass terms can then be written as

$$\mathcal{L} \supset -\begin{pmatrix} \overline{\tilde{W}}^+ & \overline{\tilde{H}}^+ \end{pmatrix}(\mathcal{M}_\chi P_L + \mathcal{M}_\chi^\dagger P_R)\begin{pmatrix} \tilde{W}^+ \\ \tilde{H}^+ \end{pmatrix}, \tag{A3}$$

where

$$\mathcal{M}_\chi = \begin{pmatrix} M_2 & \sqrt{2}\sin\beta m_W \\ \sqrt{2}\cos\beta m_W & \mu \end{pmatrix}. \tag{A4}$$

We can go to the chargino mass eigen basis $(\chi_1\chi_2)$ by making the rotations

$$P_{L,R}\begin{pmatrix} \tilde{W}^+ \\ \tilde{H}^+ \end{pmatrix} = (C_{L,R})P_{L,R}\begin{pmatrix} \tilde{\chi}_1^+ \\ \tilde{\chi}_2^+ \end{pmatrix}, \tag{A5}$$

with the rotation matrices $C_{L,R}$ given as

$$C_\alpha = \begin{pmatrix} \cos\theta_\alpha & -\sin\theta_\alpha e^{-i\gamma_\alpha} \\ \sin\theta_\alpha e^{i\gamma_\alpha} & \cos\theta_\alpha \end{pmatrix}\begin{pmatrix} e^{i\eta_\alpha} & 0 \\ 0 & e^{i\rho_\alpha} \end{pmatrix}, \tag{A6}$$

where the mixing angles and phases are [26]

$$\gamma_L = -\arg(M_2 + \mu\cot\beta)$$

$$\tan2\theta_L = \frac{\sqrt{8}m_W\sin\beta|M_2 + \mu\cot\beta|}{M_2^2 + |\mu|^2 + 2m_W^2\cos2\beta}$$

$$\gamma_R = -\arg(M_2 + \mu^*\tan\beta)$$

$$\tan2\theta_R = \frac{\sqrt{8}m_W\cos\beta|M_2 + \mu^*\tan\beta|}{M_2^2 - |\mu|^2 - 2m_W^2\cos2\beta} \tag{A7}$$

$$\eta_R = \arg[c_R(M_2 c_L + \sqrt{2}m_W\sin\beta s_L e^{i\gamma_L})$$

$$+ s_R e^{-i\gamma_R}(\sqrt{2}m_W\cos\beta c_L + \mu s_L e^{i\gamma_L})]$$

$$\rho_R = \arg[c_R(-\sqrt{2}m_W\cos\beta s_L e^{-i\gamma_L} - \mu c_L)$$

$$+ s_R e^{i\gamma_R}(-M_2 s_L e^{-i\gamma_L} + \sqrt{2}m_W\sin\beta c_L)]$$

with $0 \le \theta_\alpha \le \pi/2$ so that $M_{\alpha_1}^2 > M_{\alpha_2}^2$, and, $s_{L,R} \equiv \sin\theta_{L,R}$ and $c_{L,R} \equiv \cos\theta_{L,R}$.

The sbottom mass terms are given as cf. Eq. (5)

$$\mathcal{L} \supset -\begin{pmatrix} \tilde{b}_L^* & \tilde{b}_R^* \end{pmatrix}$$
$$\times \begin{pmatrix} m_{3LL}^2 + m_b^2 + \Delta_L^d & (v_d A_b - \mu^*\tan\beta m_b)^* \\ v_d A_b - \mu^*\tan\beta m_b & m_{\tilde{b}_R}^2 + m_b^2 + \Delta_R^d \end{pmatrix}$$
$$\times \begin{pmatrix} \tilde{b}_L \\ \tilde{b}_R \end{pmatrix}, \tag{A8}$$

where the $\Delta_{L,R}$ are the D-term contributions given as

$$\Delta^d = (T_3 - Q_{EM}\sin^2\theta_W)\cos2\beta m_Z^2. \tag{A9}$$

This is diagonalized by the rotation

$$\begin{pmatrix} \tilde{b}_L \\ \tilde{b}_R \end{pmatrix} = \begin{pmatrix} \cos\theta_{\tilde{b}} & -\sin\theta_{\tilde{b}}e^{-i\gamma_{\tilde{b}}} \\ \sin\theta_{\tilde{b}}e^{i\gamma_{\tilde{b}}} & \cos\theta_{\tilde{b}} \end{pmatrix}\begin{pmatrix} \tilde{b}_1 \\ \tilde{b}_2 \end{pmatrix}$$
$$\equiv (C_{\tilde{b}})\begin{pmatrix} \tilde{b}_1 \\ \tilde{b}_2 \end{pmatrix}, \tag{A10}$$

where the mixing angle and phase are given by

$$\tan2\theta_{\tilde{b}} = \frac{2|v_d A_b - \mu^*\tan\beta m_b|}{(m_{3LL}^2 + \Delta_L^d) - (m_{\tilde{b}_R}^2 + \Delta_R^d)},$$
$$\gamma_{\tilde{b}} = \arg(v_d A_b - \mu^*\tan\beta m_b). \tag{A11}$$

We have similar equations for stop mixing with obvious changes, in addition to the off-diagonal term now being given as: $(v_u A_t - \mu^*\cot\beta m_t)$, and the stop mixing matrix denoted as $C_{\tilde{t}}$. In our framework, owing to the smallness of the off-diagonal RL mixing term compared to $m_{3LL}^2 \sim m_0^2$, we have small stop and sbottom mixing. Furthermore, the sbottom mixing angle is negligibly small and we neglect its mixing effects. We thus have $\tilde{b}_1 \approx \tilde{b}_L$ and $\tilde{b}_2 \approx \tilde{b}_R$. The stop mixing angle, however, is not as small and so we include its effects.

To compute the interaction vertices in the SuperKM basis, one could diagonalize the 6×6 squark mass matrix. Since the off-diagonal entries in our case are small, we perform an approximate leading order diagonalization of the mass matrices shown in Eq. (5).

Focusing first on the $\tilde{b}_R\tilde{s}_L$ mixing,

$$\mathcal{L} \supset -\begin{pmatrix} \tilde{s}_L^* & \tilde{b}_R^* \end{pmatrix}\begin{pmatrix} m_{1LL}^2 + \epsilon^2 m_{2LL}^2 + m_s^2 + \Delta_L^d & (v_d A_4'\epsilon)^* \\ v_d A_4'\epsilon & m_{\tilde{b}_R}^2 + m_b^2 + \Delta_R^d \end{pmatrix}\begin{pmatrix} \tilde{s}_L \\ \tilde{b}_R \end{pmatrix}. \tag{A12}$$

This is diagonalized by the rotation

$$\begin{pmatrix} \tilde{s}_L \\ \tilde{b}_R \end{pmatrix} = \begin{pmatrix} \cos\theta_{32}^{RL} & -\sin\theta_{32}^{RL}e^{-i\gamma_{32}^{RL}} \\ \sin\theta_{32}^{RL}e^{i\gamma_{32}^{RL}} & \cos\theta_{32}^{RL} \end{pmatrix}\begin{pmatrix} \tilde{q}_2 \\ \tilde{q}_3 \end{pmatrix} \equiv (C_{\tilde{b}_R\tilde{s}_L})\begin{pmatrix} \tilde{q}_2 \\ \tilde{q}_3 \end{pmatrix}. \tag{A13}$$

The mixing angle and phase are given by

$$\tan 2\theta_{32}^{RL} = \frac{2|v_d A\epsilon|}{(m_{1LL}^2 + m_s^2 + \Delta_L^d) - (m_{\tilde{b}_R}^2 + m_b^2 + \Delta_R^d)},$$

$$\gamma_{32}^{RL} = \arg(v_d A\epsilon). \tag{A14}$$

The $\tilde{b}_R \tilde{s}_R$ mixing is given similarly. We have the mass terms

$$\mathcal{L} \supset -(\tilde{s}_R^* \quad \tilde{b}_R^*)$$
$$\times \begin{pmatrix} m_{1RR}^2 + m_s^2 + \Delta_R^d & (\epsilon m_4^2)^* \\ \epsilon m_4^2 & m_{\tilde{b}_R}^2 + m_b^2 + \Delta_R^d \end{pmatrix} \begin{pmatrix} \tilde{s}_R \\ \tilde{b}_R \end{pmatrix}, \tag{A15}$$

which is diagonalized by the rotation

$$\begin{pmatrix} \tilde{s}_R \\ \tilde{b}_R \end{pmatrix} = \begin{pmatrix} \cos\theta_{32}^{RR} & -\sin\theta_{32}^{RR} e^{-i\gamma_{32}^{RR}} \\ \sin\theta_{32}^{RR} e^{i\gamma_{32}^{RR}} & \cos\theta_{32}^{RR} \end{pmatrix} \begin{pmatrix} \tilde{q}_2 \\ \tilde{q}_3 \end{pmatrix}$$

$$\equiv (C_{\tilde{b}_R \tilde{s}_R}) \begin{pmatrix} \tilde{q}_2 \\ \tilde{q}_3 \end{pmatrix}. \tag{A16}$$

The mixing angle and phase are given by

$$\tan 2\theta_{32}^{RR} = \frac{2|\epsilon m_4^2|}{(m_{1RR}^2 + m_s^2 + \Delta_R^d) - (m_{\tilde{b}_R}^2 + m_b^2 + \Delta_R^d)},$$

$$\gamma_{32}^{RR} = \arg(\epsilon m_4^2). \tag{A17}$$

The $\tilde{d}_L \tilde{s}_L$ and $\tilde{d}_R \tilde{s}_R$ mixing terms are

$$\mathcal{L} \supset -\begin{pmatrix} \tilde{d}_{L,R}^* & \tilde{s}_{L,R}^* \end{pmatrix} \begin{pmatrix} m_1^2 + m_d^2 + \Delta_{L,R}^d & i\epsilon' m_5^2 \\ -i\epsilon' m_5^2 & m_1^2 + m_s^2 + \epsilon^2 m_2^2 + \Delta_{L,R}^d \end{pmatrix}_{LL,RR} \begin{pmatrix} \tilde{d}_{L,R} \\ \tilde{s}_{L,R} \end{pmatrix}. \tag{A18}$$

The matrices that diagonalizes these, $C_{\tilde{d}_L \tilde{s}_L}$ and $C_{\tilde{d}_R \tilde{s}_R}$ are given analogous to Eq. (A16), the angle and phase (θ_{12}^{LL}, γ_{12}^{LL}) and (θ_{12}^{RR}, γ_{12}^{RR}) given analogous to Eq. (A17), and we will not write them down explicitly. The diagonal entries are split only by $\mathcal{O}(\epsilon^2)$, and therefore this mixing is maximal in general. However, if $\epsilon' m_5^2 \ll \epsilon^2 m_2^2$, this mixing can be small.

APPENDIX B: LOOP FUNCTIONS

The $B_d \to X_s \gamma$ loop functions are given by

$$F_7^{LL}(x) = \left(\frac{x(7 - 5x - 8x^2)}{36(x-1)^3} + \frac{x^2(3x-2)}{6(x-1)^4} \ln x \right), \qquad F_8^{LL}(x) = \left(\frac{x(2 + 5x - x^2)}{12(x-1)^3} - \frac{3x^2}{6(x-1)^4} \ln x \right),$$

$$F_7^{RL}(x) = \left(\frac{5 - 7x}{6(x-1)^2} + \frac{x(3x-2)}{3(x-1)^3} \ln x \right), \qquad F_8^{RL}(x) = \left(\frac{1 + x}{2(x-1)^2} - \frac{x}{(x-1)^3} \ln x \right), \tag{B1}$$

$$\tilde{F}_7^{LL}(x) = \left(\frac{x(3 - 5x)}{12(x-1)^2} + \frac{x(3x-2)}{6(x-1)^3} \ln x \right), \qquad \tilde{F}_8^{LL}(x) = \left(\frac{x(3 - x)}{4(x-1)^2} - \frac{x}{2(x-1)^3} \ln x \right).$$

$$F_4(x) = \frac{x^2 - 1 - 2x \ln x}{2(x-1)^3} \qquad F_{\tilde{g}}(x) = -\frac{5x^2 - 18x + 13 + (9 - x) \ln x}{3(x-1)^3} \tag{B2}$$

The SM box functions are given by

$$S_0(x) = \frac{4x - 11x^2 + x^3}{4(1-x)^2} - \frac{3x^3 \ln x}{2(1-x)^3}, \qquad S_0(x_1, x_2) = \frac{x_1 x_2}{4} \left\{ \frac{x_1^2 - 8x_1 + 4}{(x_1 - x_2)(x_1 - 1)^2} \ln x_1 + \frac{x_2^2 - 8x_2 + 4}{(x_2 - x_1)(x_2 - 1)^2} \ln x_2 - \frac{3}{(x_1 - 1)(x_2 - 1)} \right\}. \tag{B3}$$

The charged-Higgs and chargino box functions are given by

$$Y_1(r_\alpha, r_\beta, s_i, s_j) = \frac{r_\alpha^2}{(r_\beta - r_\alpha)(s_i - r_\alpha)(s_j - r_\alpha)} \ln r_\alpha + \frac{r_\beta^2}{(r_\alpha - r_\beta)(s_i - r_\beta)(s_j - r_\beta)} \ln r_\beta$$
$$+ \frac{s_i^2}{(r_\alpha - s_i)(r_\beta - s_i)(s_j - s_i)} \ln s_i + \frac{s_j^2}{(r_\alpha - s_j)(r_\beta - s_j)(s_i - s_j)} \ln s_j,$$
$$Y_2(r_\alpha, r_\beta, s_i, s_j) = \sqrt{s_i s_j}\Bigg[\frac{r_\alpha}{(r_\beta - r_\alpha)(s_i - r_\alpha)(s_j - r_\alpha)} \ln r_\alpha + \frac{r_\beta}{(r_\alpha - r_\beta)(s_i - r_\beta)(s_j - r_\beta)} \ln r_\beta$$
$$+ \frac{s_i}{(r_\alpha - s_i)(r_\beta - s_i)(s_j - s_i)} \ln s_i + \frac{s_j}{(r_\alpha - s_j)(r_\beta - s_j)(s_i - s_j)} \ln s_j \Bigg].$$

(B4)

from which various limiting cases can be obtained.

The gluino box integrals are given as

$$I_4 \equiv I_4(M_{\tilde{g}}^2, M_{\tilde{g}}^2, m_{\tilde{b}_R}^2, m_{\tilde{b}_R}^2) = \int \frac{d^4 p}{(2\pi)^4} \frac{1}{(p^2 - M_{\tilde{g}}^2)(p^2 - M_{\tilde{g}}^2)(p^2 - m_{\tilde{b}_R}^2)(p^2 - m_{\tilde{b}_R}^2)},$$
$$\tilde{I}_4 \equiv \tilde{I}_4(M_{\tilde{g}}^2, M_{\tilde{g}}^2, m_{\tilde{b}_R}^2, m_{\tilde{b}_R}^2) = \int \frac{d^4 p}{(2\pi)^4} \frac{p^2}{(p^2 - M_{\tilde{g}}^2)(p^2 - M_{\tilde{g}}^2)(p^2 - m_{\tilde{b}_R}^2)(p^2 - m_{\tilde{b}_R}^2)},$$

(B5)

which we evaluate numerically using LoopTools [36] in Mathematica.

[1] A. G. Cohen, D. B. Kaplan, and A. E. Nelson, Phys. Lett. B **388**, 588 (1996).
[2] A. Pomarol and D. Tommasini, Nucl. Phys. **B466**, 3 (1996).
[3] R. Barbieri, G. R. Dvali, and L. J. Hall, Phys. Lett. B **377**, 76 (1996); R. Barbieri, L. J. Hall, and A. Romanino, Phys. Lett. B **401**, 47 (1997).
[4] G. Degrassi, P. Gambino, and G. F. Giudice, J. High Energy Phys. 12 (2000) 009; M. Carena, D. Garcia, U. Nierste, and C. E. Wagner, Phys. Lett. B **499**, 141 (2001).
[5] S. Bertolini, F. Borzumati, A. Masiero, and G. Ridolfi, Nucl. Phys. **B353**, 591 (1991).
[6] J. S. Hagelin, S. Kelley, and T. Tanaka, Nucl. Phys. **B415**, 293 (1994).
[7] L. J. Hall, V. A. Kostelecky, and S. Raby, Nucl. Phys. **B267**, 415 (1986); F. Gabbiani and A. Masiero, Nucl. Phys. **B322**, 235 (1989); F. Gabbiani, E. Gabrielli, A. Masiero, and L. Silvestrini, Nucl. Phys. **B477**, 321 (1996); M. Misiak, S. Pokorski, and J. Rosiek, Adv. Ser. Dir. High Energy Phys. **15**, 795 (1998).
[8] G. L. Kane, P. Ko, H. B. Wang, C. Kolda, J. H. Park, and L. T. Wang, Phys. Rev. D **70**, 035015 (2004); K. Agashe and C. D. Carone, Phys. Rev. D **68**, 035017 (2003).
[9] CDF Collaboration, T. Affolder et al., Phys. Rev. Lett. **84**, 5704 (2000); C. Rott, hep-ex/0410007.
[10] Particle Data Group Collaboration, S. Eidelman et al., Phys. Lett. B **592**, 1 (2004).
[11] G. C. Branco, G. C. Cho, Y. Kizukuri, and N. Oshimo, Phys. Lett. B **337**, 316 (1994);Nucl. Phys. **B449**, 483 (1995).

[12] G. Buchalla, A. J. Buras, and M. E. Lautenbacher, Rev. Mod. Phys. **68**, 1125 (1996).
[13] D. Becirevic et al., Nucl. Phys. **B634**, 105 (2002).
[14] P. Ko, J. H. Park, and G. Kramer, Eur. Phys. J. C **25**, 615 (2002).
[15] A. J. Buras and R. Fleischer, Adv. Ser. Dir. High Energy Phys. **15**, 65 (1998).
[16] L. Randall and S. F. Su, Nucl. Phys. **B540**, 37 (1999).
[17] We use the (ICHEP 2004) average from CLEO, *BABAR* and Belle compiled by the Heavy Flavor Averaging group http://www.slac.stanford.edu/xorg/hfag/.
[18] Y. Grossman, Y. Nir, and M. P. Worah, Phys. Lett. B **407**, 307 (1997).
[19] G. C. Branco, L. Lavoura, and J. P. Silva, *CP Violation* (Clarendon Press, Oxford 1999).
[20] K. Anikeev et al., hep-ph/0201071.
[21] A. J. Buras, hep-ph/9806471.
[22] A. J. Buras and M. Munz, Phys. Rev. D **52**, 186 (1995).
[23] A. J. Buras, M. Misiak, M. Munz, and S. Pokorski, Nucl. Phys. **B424**, 374 (1994).
[24] K. G. Chetyrkin, M. Misiak, and M. Munz, Phys. Lett. B **400**, 206 (1997); **425**, 414E (1998).
[25] B. Grinstein, R. P. Springer, and M. B. Wise, Phys. Lett. B **202**, 138 (1988).
[26] D. A. Demir and K. A. Olive, Phys. Rev. D **65**, 034007 (2002).
[27] R. Barbieri and G. F. Giudice, Phys. Lett. B **309**, 86 (1993).
[28] A. Ali, H. Asatrian, and C. Greub, Phys. Lett. B **429**, 87 (1998); A. L. Kagan and M. Neubert, Eur. Phys. J. C **7**, 5 (1999).

[29] A. L. Kagan and M. Neubert, Phys. Rev. D **58**, 094012 (1998).

[30] S. Bertolini, F. Borzumati, and A. Masiero, Nucl. Phys. **B294**, 321 (1987); R. Barbieri and G. F. Giudice, Phys. Lett. B **309**, 86 (1993); P. L. Cho, M. Misiak, and D. Wyler, Phys. Rev. D **54**, 3329 (1996); .J. L. Hewett and J. D. Wells, Phys. Rev. D **55**, 5549 (1997).

[31] Belle Collaboration, S. Nishida *et al.*, Phys. Rev. Lett. **93**, 031803 (2004).

[32] *BABAR* Collaboration, B. Aubert *et al.*, Phys. Rev. Lett. **93**, 021804 (2004).

[33] A. L. Kagan and J. Rathsman, hep-ph/9701300.

[34] M. Beneke, G. Buchalla, M. Neubert, and C. T. Sachrajda, Nucl. Phys. **B606**, 245 (2001).

[35] M. Beneke and M. Neubert, Nucl. Phys. **B675**, 333 (2003).

[36] T. Hahn and M. Perez-Victoria, Comput. Phys. Commun. **118**, 153 (1999).